LHCb/2002-045
TRIG
August 15, 2002

The use of the TT1 tracking station in the Level-1 trigger

H. Dijkstra, T. Schietinger, F. Teubert and M. Witek

CERN, EP division

D. Wiedner

Physics Institute, University of Heidelberg

Abstract

We present the algorithms that form the basis of an efficient (mini-)Level-1 trigger: the VELO tracking including primary vertex finding, TT1 tracking and matching to VELO track seeds, with determination of the transverse momentum, and finally a simple decision logic based on the impact parameters and transverse momenta of two selected tracks in the event. For the TT1 tracking station, two implementations are considered, a straw-tube/silicon hybrid version and a full-silicon design. The inclusion of the TT1 tracking station improves dramatically the Level-1 trigger performance with respect to the algorithm described in the Technical Proposal. We arrive at the conclusion that a full-silicon implementation of this tracking chamber performs significantly better than the hybrid version.

Contents

1 Introduction

The large $b\bar{b}$ cross section (≈ 0.5 mb) in proton-proton collisions at $\sqrt{s} \approx 14$ TeV makes the LHC collider an ideal laboratory for the study of the b-quark. LHCb is designed to operate at an average luminosity of 2×10^{32} cm^{-2}s^{-1} such that events are dominated by single proton-proton interactions and the occupancy in the detector remains low.

Probably one of the most critical element of LHCb is the trigger system. The $b\bar{b}$ cross section mentioned above is just a small fraction of the total "visible" cross section in LHCb (≈ 60 mb). Moreover, the total $c\bar{c}$ cross section is more than one order of magnitude larger than the $b\bar{b}$ cross section and the amount of "interesting" $b\bar{b}$ events is just a small fraction of the total cross section, (less than ≈ 1 μb).

The lower level triggers (Level-0 and Level-1), will aim at rejecting non-b events. They will merely rely on two main features of the b-hadron decays: significant transverse momentum of the daughter particles as a consequence of the high b-quark mass and long lifetime. These two levels will aim at reducing the 40 MHz input rate to 40 kHz.

The first trigger level (Level-0), based on calorimeter and muon chamber information, will reduce the event rate to 1 MHz by requiring a muon, an electron or a hadron with a transverse momentum or energy above some threshold. In addition, a pile-up veto system is foreseen: two dedicated silicon disks located upstream of the vertex locator (VELO) will be used to reconstruct the longitudinal position of the interaction vertices and reject events with two or more such vertices. After this cut, the event rate is approximately 10 MHz, with more than 90% single interactions and the requirements on p_T (E_T) may be relaxed. The Level-0 decision will take 4 μs during which the data will be kept in the pipeline of the front-end electronics.

The second trigger level (Level-1) achieves a further reduction in rate by a factor of 25. The Level-1 buffer will reside on off-detector electronics, with a depth allowing for a maximum latency of 1.7 ms. After a Level-1 accept, the zero-suppressed data are transferred to the data acquisition (DAQ) system and the full event buffer made available to the high level software triggers (Level-2 and Level-3).

The Level-1 algorithm described in the Technical Proposal (TP) [1] assigns a b-event probability using displaced vertices found in the VELO. The performance of this algorithm on the most recent Monte Carlo samples is not as good as quoted in the TP due to the addition of pile-up events, the new tuning of the PYTHIA generator [2] and a more realistic description of the detector. For instance, at 4% retention of minimum-bias events after Level-0 (i.e. 40 kHz Level-1 output rate), the efficiency for offline selected $B^0_d \to \pi^+\pi^-$ events is only 30% (to be compared with the 45% quoted in the TP).

The main limitation of the algorithm is the lack of p_T information that would allow the trigger to differentiate B decays from other sources of tracks with large impact parameter. Moreover, the significance of the impact parameter is not known: tracks with low momentum and thus large multiple-scattering angle cannot be distinguished from real large-impact-parameter tracks. Two options for overcoming these limitations have been studied:

- *Link Level-1 tracks to Level-0 objects:* Tracks reconstructed in the VELO with large impact parameter are extrapolated to the calorimeters (HCAL and ECAL) and the muon chambers and matched to energy deposits found by the Level-0 trigger. For instance, the efficiency to match one of the two pions with an HCAL cluster in $B^0_d \to \pi^+\pi^-$ events is about 78%, while the efficiency to match one of the two muons in $B^0_d \to J/\psi(\mu^+\mu^-)K^0_S$ events is about 98%. Using the measurement of p_T (E_T) from Level-0 the performance of the Level-1 algorithm is improved significantly. At 40 kHz output rate the efficiency for $B^0_d \to \pi^+\pi^-$ events is around 60%, while for $B^0_d \to J/\psi(\mu^+\mu^-)K^0_S$ it is close to 90% (normalized to offline-reconstructable events). As the information from Level-0 already exists, and the amount of data to be sent to the Level-1 CPU-farm is small, this is a straightforward improvement. This approach to enhance the Level-1 trigger is also called *Super-Level-1* [3].

- *Obtain a rough estimate of the transverse momentum:* If a small fraction of the magnetic field (about 10% of the peak value) is available in the tracking station just in front of the magnet (TT1), a measurement of the momentum with a relative precision of about 20% is feasible. Because the matching between VELO tracks and TT1 digits is much more efficient than in the previous case, the performance is even better. At 40 kHz output rate the signal efficiency for $B^0_d \to \pi^+\pi^-$ events is around 80%. Even more interesting is the possibility to work with significantly lower Level-1 output rates (20 kHz) while still keeping high signal efficiency. The drawbacks are an increase of the Level-1 event size by about 30% and the necessary redesign of the detector to handle the magnetic field in this area. This option has become known under the name *mini-Level-1* [4].

Pursuing both approaches is desirable for an optimal trigger performance as well as for the robustness of the system. This note will demonstrate the validity of the second approach, i.e. the use of the TT1 tracking station in the Level-1 trigger.

Level-0 keeps 6% of the generated minimum-bias events, only 4% of which are then selected by Level-1. The events triggered by Level-1 are therefore to be found in the tails of the tails of the distributions of the relevant variables, and an as realistic as possible simulation of the detector is of paramount importance. In Sec. 2 the algorithms used to digitize the VELO clusters, reconstruct the VELO tracks and the primary vertex are briefly described together with their performance. In Sec. 3 we present the algorithm used to find clusters in TT1 and to match them to the VELO tracks. Here we consider two technology options for TT1: an implementation in full silicon and a mixed implementation with a cross-shaped inner part made of silicon and an outer part consisting of straw tubes, following the design of the downstream tracking stations (ST1–ST3). In both configurations, TT1 consists of four layers (x, u, v, x), with a gap between the first and the last two layers. Finally, a possible Level-1 decision logic based on VELO–TT1 tracks is described in Sec. 4, along with the performance curves of such an algorithm for the two TT1 options.

2 Reconstruction of VELO tracks and the primary vertex

The VELO detector as described in the Technical Design Report [5] and implemented in the database v243, is used to reconstruct tracks and a list of primary vertices. The algorithm used in this note reconstructs three-dimensional tracks by first combining the information of the r-sensors and the ϕ-sensors to obtain 3D space points and then searching for straight lines through them. This approach is expected to be more robust against possible misalignments as one can always correct the 3D coordinates with pre-tabulated alignment constants. The drawback, though, is an increase in combinatorics which makes it very difficult to stay within the allocated Level-1 maximum latency time of 1.7 ms. The algorithm can probably be used for the high-level triggers (Level-2 and Level-3) but more work on the speed optimization is needed.

The VELO tracks are reconstructed using binary cluster resolution taking into account the Level-1 buffer requirements [6]. We describe in Sec. 2.1 the procedure used to obtain clusters. The tracking algorithm and its performance are presented in Secs. 2.2 and 2.3, and Sec. 2.4 gives a description of the algorithm used for the reconstruction of the primary vertices.

2.1 VELO digits and clusters

2.1.1 Digitization

A search for GEANT energy deposits above a treshold (30 keV) in a single strip is performed. Due to the Level-1 buffer requirements, only up to two consecutive strips with energy deposits above the treshold are used to form a digit. The centre of the strip, or the average of the centres, is used for the space coordinates (binary resolution). Note that no use of analog information is made.

2.1.2 Clusterization

Clusters are built from the list of digits in the Level-1 buffer allowing up to two consecutive digits to form a cluster. Each cluster provides a coordinate measurement which is the average of the digit's coordinates and an error computed from the strip pitch and the number of strips contributing to the cluster. Each r-cluster is extrapolated to the z-position of the neighbouring ϕ-sensor, assuming the origin of the track to be at (0,0,0), and matched with all ϕ-clusters in the corresponding sector to form a set of three-dimensional *point measurements*. This list of point measurements is the input to the tracking algorithm. The resolution in the xy-plane is shown in Fig. 1. The average resolution, convoluting all strip pitches, is around 14 μm.

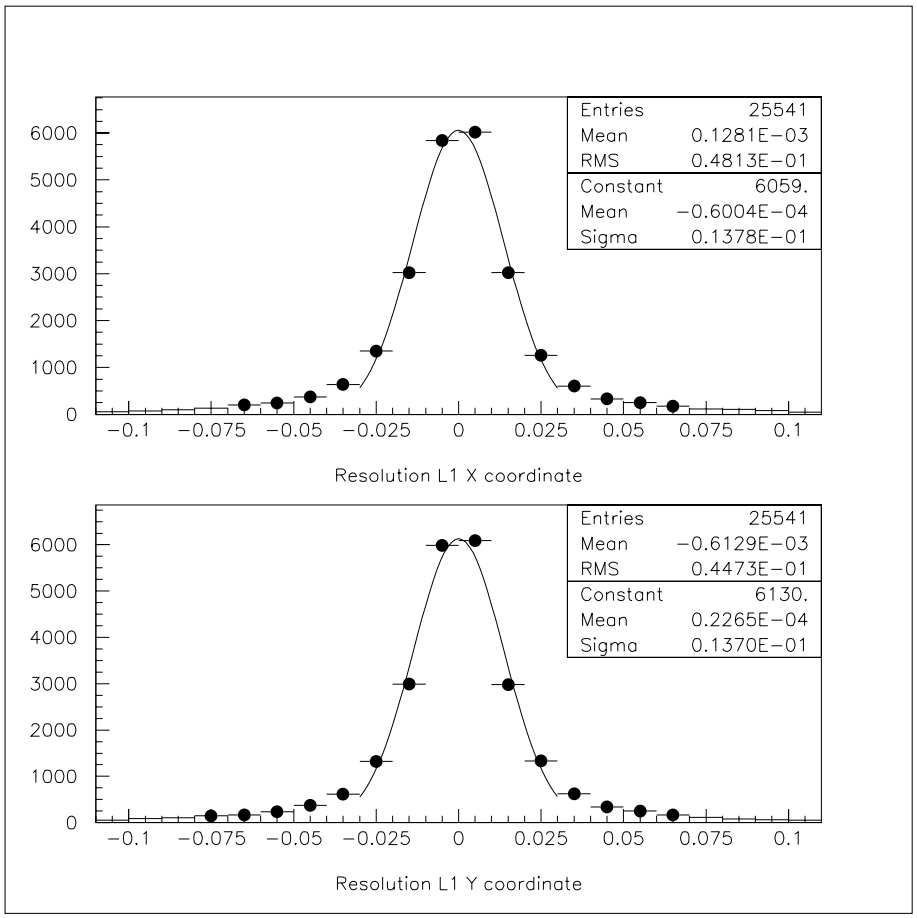

Figure 1: Level-1 clusters resolution in the xy-plane (in mm).

2.2 Standalone tracking using VELO clusters

The algorithm first searches for triplets of point measurements starting from the downstream stations. Three point measurements from consecutive stations are considered to be a triplet if the point in between lies within 3σ of the interpolation between the other two points. A triplet is accepted as a track seed if the point of closest approach between its extrapolation and the beam line has coordinates within ± 400 mm in z and ± 10 mm in the xy-plane.

If a track seed is found, it is extrapolated to the next station upstream. If a point measurement is located within 3σ, the track parameters are updated, using only the last three measurements, i.e., the ones closest to the primary vertex. The procedure continues until the extrapolation runs out of the VELO acceptance. The algorithm may skip up to three stations in the extrapolation of the triplets to allow for possible inefficiencies of the sensors. After every successful track finding, a cleaning procedure is applied to avoid clone tracks: if the track has the complete r or ϕ projection in common with a previously found track, the shorter of the two is removed or, if the lengths are equal, the one having the worse χ^2. Similarly, if two tracks share more than 30% of their digits (the same digit can be part of different clusters), the one

Table 1: Standalone VELO tracking reconstruction efficiency, clone and ghost rate for tracks from B meson decays, and for all tracks in the acceptance.

	efficiency	clone rate	ghost rate
b-tracks ($\eta > 2.2$)	$(98.1 \pm 0.3)\%$		
tracks in acc. ($\eta > 2.2$)	$(98.3 \pm 0.1)\%$		
tracks in acc.	$(97.2 \pm 0.1)\%$		
		$(1.5 \pm 0.1)\%$	$(13.3 \pm 0.1)\%$

with the worse χ^2 is removed. Once a track has been identified in this manner, its constituent measurement points are not used in the reconstruction of further tracks. After the search for forward tracks is completed, the algorithm is applied to look for backward tracks in the same way.

2.3 Tracking performance

The performance of the VELO standalone 3D tracking algorithm is evaluated in terms of efficiencies, ghost and clone rates. The acceptance is defined to be all tracks that have enough MC hits in the VELO to form at least three point measurements, at least three MC hits in the seeding stations (ST1–ST3), and a track origin z-coordinate within ± 100 mm (in the simulation). A reconstructed track is considered to be matched with a MC track if at least 70% of the digits are in common.

The performance was evaluated based on these definitions using 1000 $\mathrm{B}^0_\mathrm{d} \to \pi^+\pi^-$ events (database v243r1p1) and is summarized in Table 1. An average of 55 forward tracks are reconstructed per event, only 23 of which are in the acceptance as defined above. The efficiency for reconstructing tracks in the acceptance is $(97.2 \pm 0.1)\%$, with a negligible clone rate of $(1.5 \pm 0.1)\%$. Some $(13.3 \pm 0.1)\%$ of the reconstructed tracks are ghost tracks.

In Fig. 2 we show the efficiency as functions of the pseudorapidity η and the transverse momentum p_T of the track. The drop in efficiency at low η is due to the hypothesis that the origin of the track is at (0,0,0) when the r-sensors and ϕ-sensors are matched to build the three-dimensional point measurements. This assumption is often not valid for tracks with $\eta < 2.2$, as the interaction point has a spread of 5.3 cm along the beam axis. This problem could be solved by obtaining a preliminary measurement of the primary-vertex position from the tracks already found at large η, or/and using the information from the previous trigger levels. In any case, the performance of the tracking algorithm is more than adequate for the studies presented in this note.

The parameters describing a track are determined from a linear fit to the three point measurements closest to the primary vertex. Using all measurements in the track would result in a worse description of the track because of the effects of random multiple scattering. Figure 3 shows the impact parameter resolution as a function

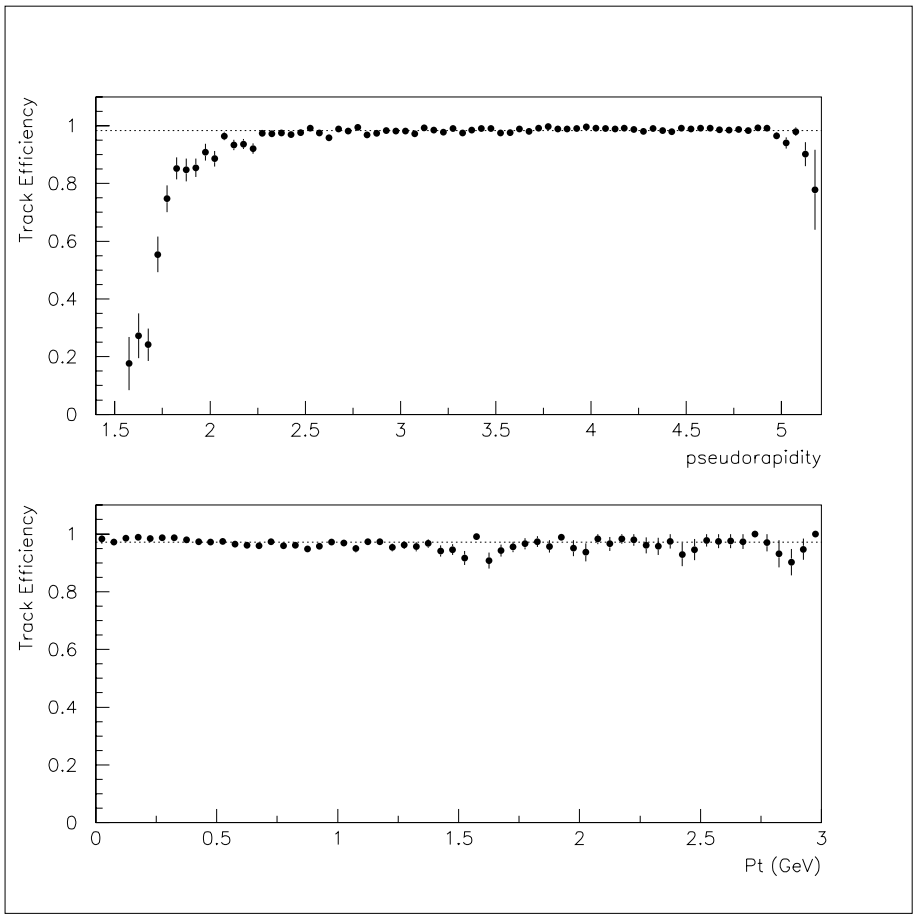

Figure 2: The tracking efficiency as a function of pseudorapidity η (upper plot) and as a function of transverse momentum p_T (lower plot).

of the transverse momentum p_T. The impact parameter is calculated with respect to the MC primary vertex in this case. The resolution can easily be parameterized as a function of p_T and the distance between the measured space-points and the MC primary vertex (see Ref. [7] for more details). As can be seen in Fig. 3 the agreement between this parameterization and the real impact-parameter uncertainty is very good. Note that the resolution is expected to be worse than what can be done offline due to the VELO clusters digital resolution. Notice, however, that what is plot in Fig. 3 is the RMS of the distribution and not the result of a gaussian fit. The impact-parameter significance for b-tracks computed using this parameterization is shown in Fig. 4.

2.4 Reconstruction of the primary vertex

2.4.1 Seed finding

Even after the Level-0 pile-up veto a significant fraction of the events still have more than one primary vertex. Hence, the primary vertex algorithm used in this

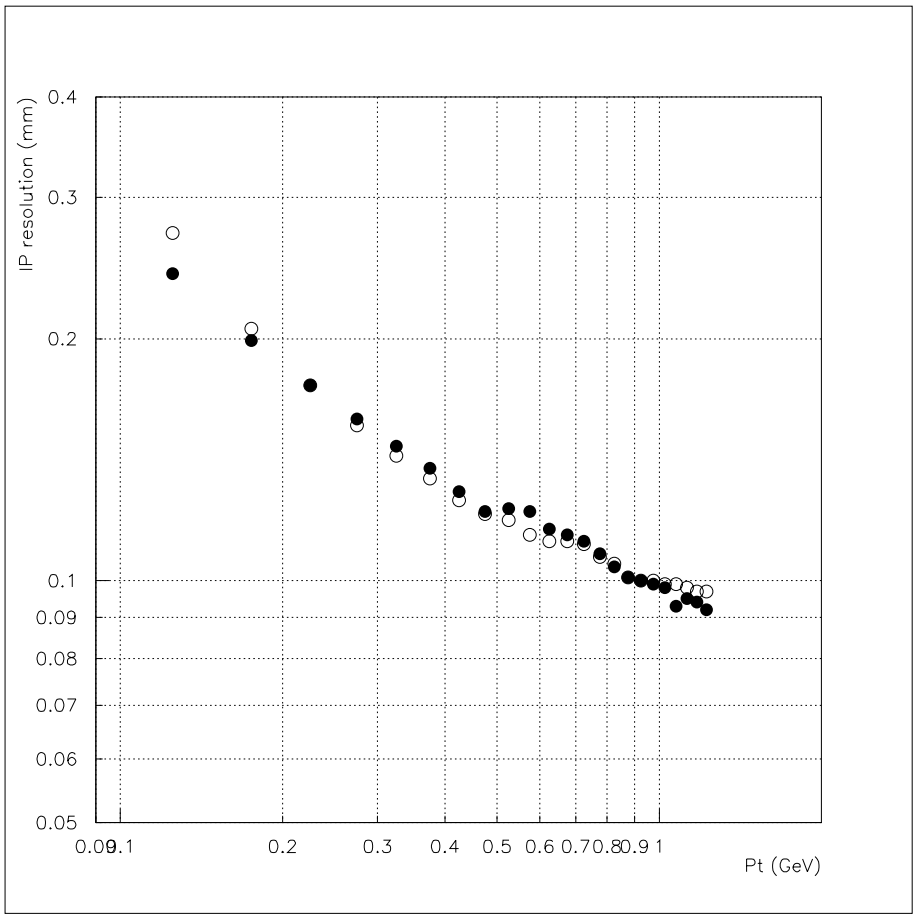

Figure 3: Impact parameter resolution as a function of p_T. The full points are the RMS of the diference between the measured impact parameter and the MC truth in bins of p_T. The open points correspond to the average error from the parameterization of reference [7] in bins of p_T.

note initially performs a search for multiple primary vertices by histogramming the z-position of the point of closest approach to the beam line for each track. The peak containing the most entries is used as primary-vertex seed, and the tracks in a region of ± 4 mm are used as input to the fit procedure employed to compute the position of the primary vertex. If a clearly separated second peak is found in the histogram containing at least 20% of the remaining tracks, a second primary vertex is determined in the same way.

2.4.2 Fit procedure

Consider a track with unit direction vector $\mathbf{s}$, passing through a point $\mathbf{a}$. Its three-dimensional impact-parameter vector $\mathbf{d}_0$ with respect to the primary vertex position $\mathbf{p}$ is given by

$$\mathbf{d}_0 = (\mathbf{a} - \mathbf{p}) - \mathbf{s} \cdot [(\mathbf{a} - \mathbf{p}) \cdot \mathbf{s}] = \mathbf{s} \times [(\mathbf{a} - \mathbf{p}) \times \mathbf{s}].$$

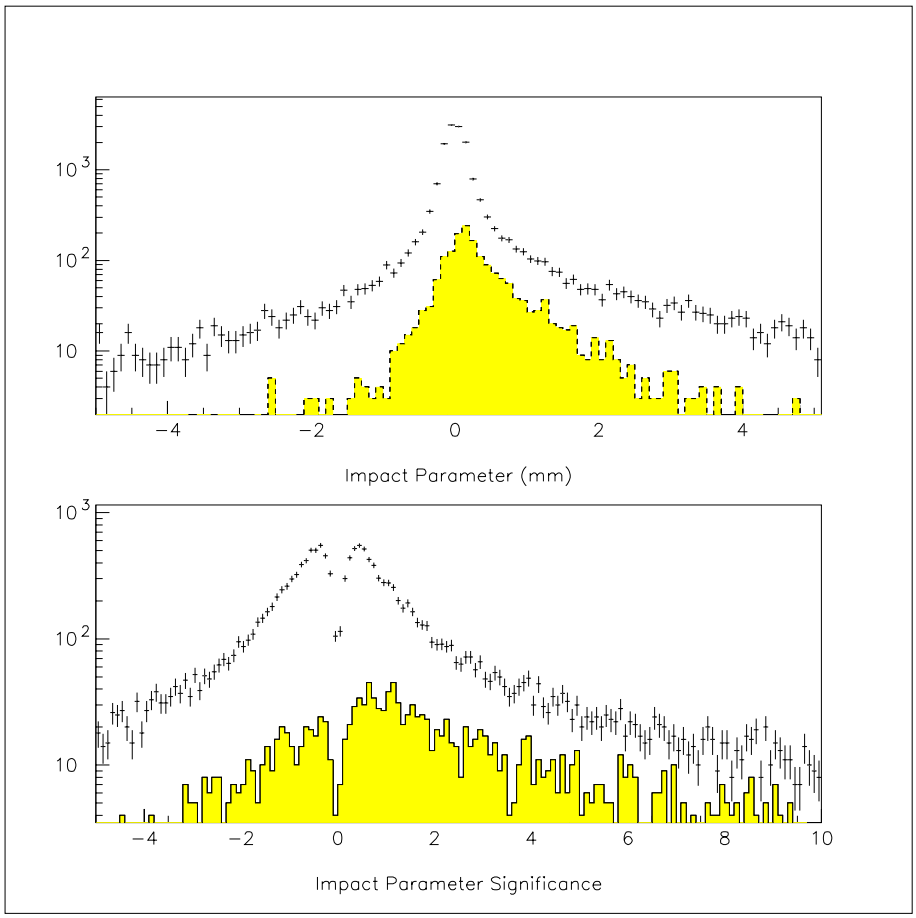

Figure 4: Top: Impact parameter distribution for all tracks and for b-tracks (hatched histogram). Bottom: Impact-parameter significance for all tracks and b-tracks (hatched histogram).

The primary vertex position is estimated by minimizing the following expression with respect to **p**:

$$\chi^2 = \sum_{i=1}^{N_{\mathrm{PV}}} \left(\frac{|\mathbf{d}_0|^2}{\sigma_d^2} \right)_i , \tag{1}$$

where the sum extends over a set of tracks that has been preselected according to the seed-finding mechanism described above. σ_d is the uncertainty on $|\mathbf{d}_0|$, estimated from the parameterization mentioned in Sec. 2.3. Although in principle one could arrive at a better expression for χ^2 by using the full covariance matrix of the track (if it were available), in practice, since the impact-parameter resolution is dominated by multiple scattering, correlations are small and hence this would give little improvement. As the p_T of the track is not known at this stage the average p_T of 400 MeV is assigned to compute the impact-parameter significance. The χ^2-minimization can be performed by Newtonian iteration, see Ref. [7] for more details.

The resolution obtained using this algorithm is shown in Fig. 5. The resolution in

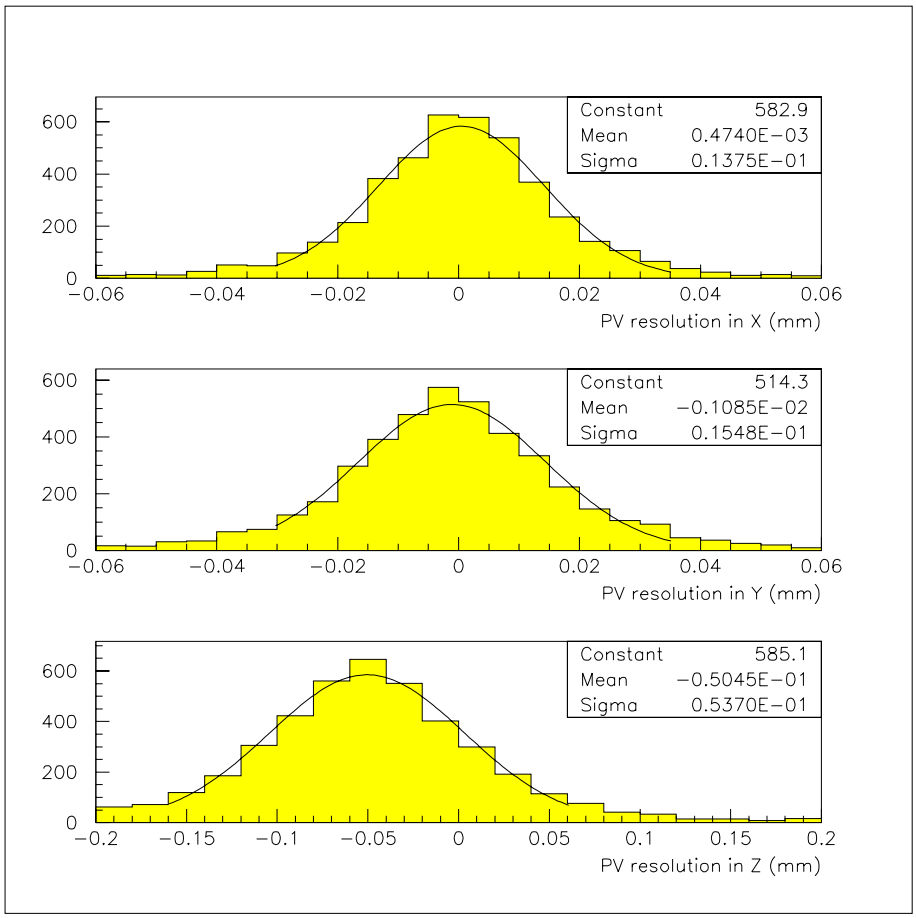

Figure 5: Primary vertex resolution in xy and z (in mm).

the xy-plane is 14 μm, while in the z-direction it is 54 μm. Note that the resolution of the same algorithm used offline, i.e. with access to analog VELO clusters resolution and p_T measured in the tracking stations, would be 8 μm in the xy-plane and 32 μm in z. (The obvious shift in the z-position of the primary vertex is due to an inconsistency in the calculation of the MC truth z-position, and has no effect on the results shown in this note.)

The efficiency to find the primary vertex is 100% by definition as long as there is at least one track reconstructed in the VELO, which is always the case after Level-0. About 10% of the events that trigger Level-0 are found to have more than one primary vertex by this algorithm. The resolution on the position of the second vertex is worse by about 20%.

3 TT1 matching

The goal of the track reconstruction in TT1 at Level-1 is to obtain a momentum estimate for tracks with high impact parameter found in the VELO. The successful matching of TT1 hits to VELO tracks requires taking account of the effect of multiple scattering (12% X_0 between VELO and TT1) and the influence of the magnetic field between the two detectors. Two technology options for TT1 are considered: an implementation in full silicon and a mixed implementation with a cross-shaped inner part made of silicon (following the LHCb Inner Tracker design) and an outer part consisting of straw tubes (following the LHCb T2 Outer Tracker design [8]). We first give a brief overview over the two configurations for TT1.

3.1 TT1 design and layout

In both configurations, TT1 consists of four layers (x, u, v, x), with a gap between the first and the last two layers.

3.1.1 Full-silicon TT1

For the simulation of the detector containing the full-silicon TT1 database v243r1p1 was used. In that description, the two halves of TT1 are split by 30 cm. The x- and stereo layers of each half are separated by 11 mm, and some y-segments are displaced in z by 22 and 70 mm (see Fig. 6). The Silicon sensors are 0.4 mm thick and the strip pitch is 0.24 mm. The dimension of the sensors in the simulation is 78 mm×110 mm, hence the intrinsic segmentation in the y-coordinate is 110 mm. For a more detailed description of the layout see Ref. [9].

3.1.2 Hybrid straw-silicon TT1

The mixed solution for TT1 consists of an Inner Tracker part in silicon and an Outer Tracker part equipped with straw tubes. It is modeled by database v243r3. Here, the split between the two halves is 30 cm for the silicon and 50 cm for the straw tubes (Fig. 7). The x- and stereo layers of each half are separated by 46.8 mm in the case of the straw tubes, by 11 mm in the inner silicon part. In the inner part, the left and right "wings" of the detector are displaced in z by 48 mm. The straw tubes are 328(481) mm long, and the pitch is 5.25 mm. Hence, the intrinsic segmentation in the y-coordinate varies between 328 mm and 481 mm. See also Ref. [10].

3.2 TT1 clusterization

In the case of the silicon design, the clusterization procedure is simple since the relatively large strip pitch of 240 μm predominantly results in single hit clusters. This binary resolution is expected to be about 70 μm. The distribution of the distance between the strip position and the track trajectory is shown in Fig. 8.

In the case of the straw-tube (Outer Tracker) technology, the double layer structure in each projection and the left-right ambiguity for each hit must be taken into

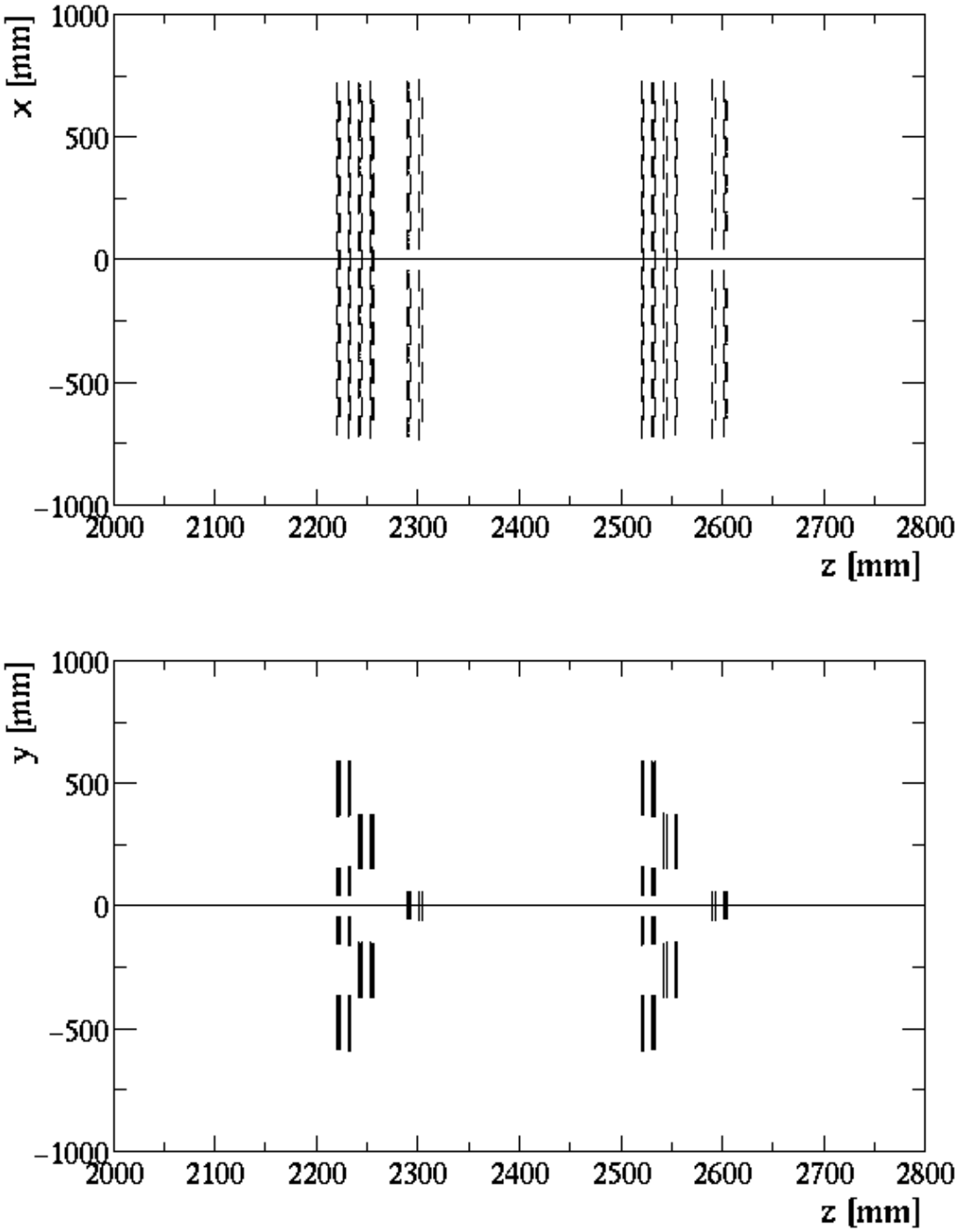

Figure 6: Distribution of Monte Carlo hits in the full-silicon version of TT1 for illustration of its layout (see also Ref. [9]).

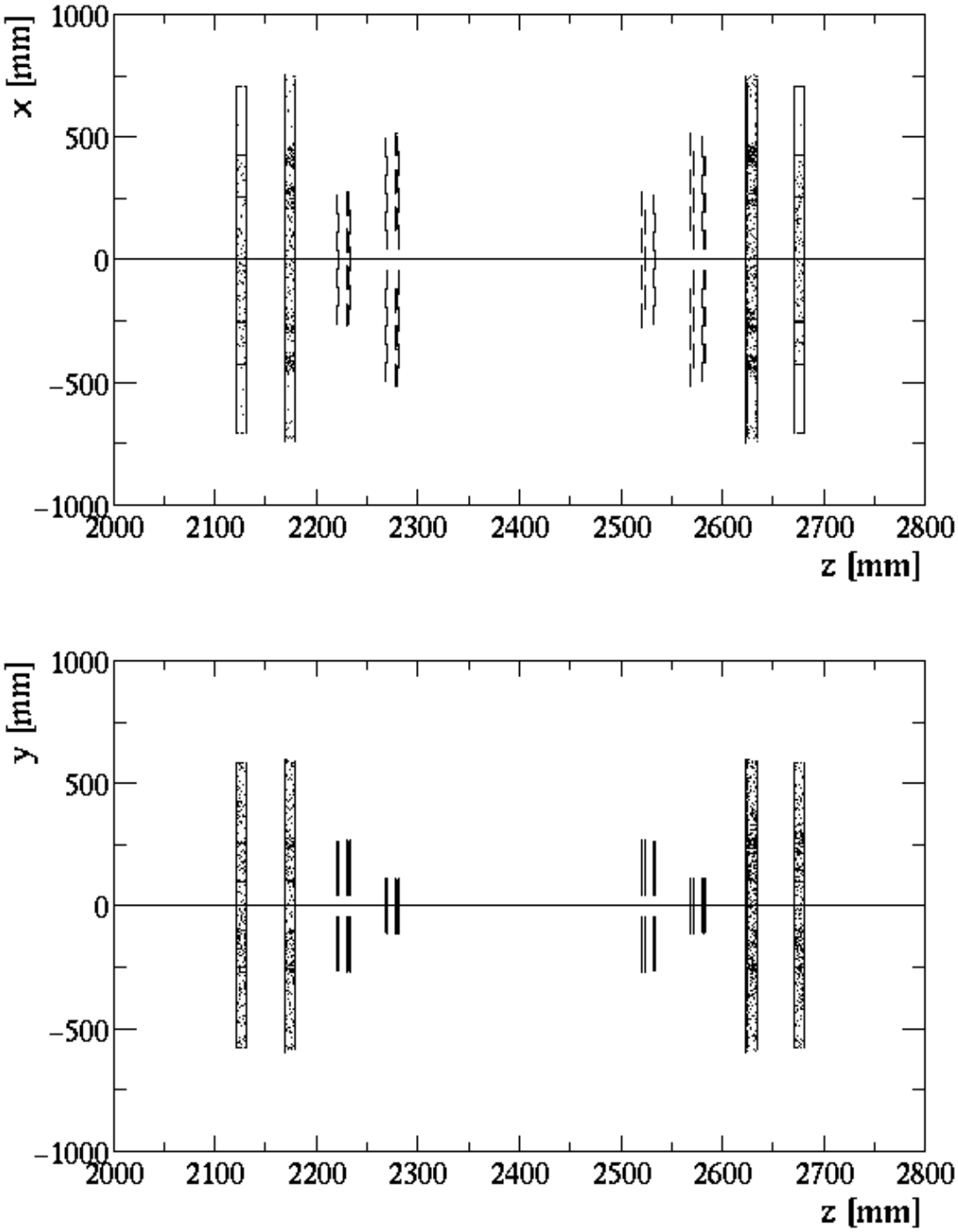

Figure 7: Distribution of Monte Carlo hits in the hybrid straw-silicon version of TT1 for illustration of its layout (see also Ref. [10]).

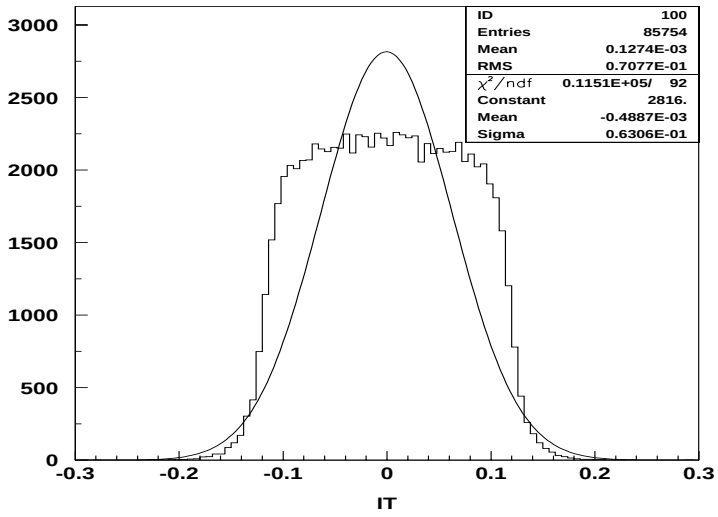

Figure 8: The binary resolution for the silicon design (in mm).

account. The utilization of the information from the straw tubes at the trigger level requires a dedicated hardware-based preprocessing. This preprocessing must be compatible with a parallel hardware implementation in order to be executed online. A software emulation of such a processing has been developed, and is briefly outlined in the following.

The algorithm combines detector hits from two layers and returns zero-suppressed track information. For each Outer Tracker module consisting of two layers of straw tubes (128 channels), the algorithm scans the detector for hits. For every hit found the neighboring channels in both layers are checked for hits. In case of a double hit (one hit per layer), the position of the track is calculated from the two measured drift times (mean of the radii of the isochrones taking into account the cell offsets) and is sent together with the channel ID of one of its constituent cells. The ambiguity is solved according to the illustration in Fig. 9a. If only one single hit in the two layers is found, the drift time and the channel address are sent to the L1-Trigger. The ambiguity remains unsolved, see Fig. 9b. The algorithm also accounts for larger track angles in the outer regions of the detector ($> 14^\circ$ in x). These double hits have an unsolved ambiguity shown in Fig. 9c. For high occupancies, hits from different particles will sometimes be combined to fake double hits. The percentage of fake double hits is of the order of the occupancy (some 5%). A comparison of the hits with the Monte Carlo tracks shows that for 74% of all the hits coming from reconstructed tracks the ambiguity is solved, whereas 24% single hits and 2% hits under large angle remain with unsolved ambiguities. The algorithm improves the hit resolution from an assumed 400 μm resolution of a single straw to 320 μm for the combined hits. The clusterization procedure reduces the data from the straw tubes to about 62% of the initial size. Including zero suppression a total data volume of

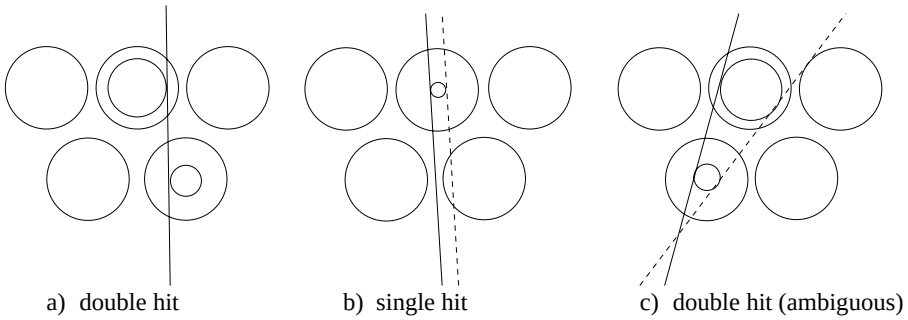

Figure 9: The three cases considered when searching for hits in the straw tubes (see text for details).

0.3 GB/s for the entire TT1 station is expected.

The performance of the clusterization procedure was further checked with respect to possible inefficiencies and detector resolutions. To this end we compare, for a given track, the number of straw hits caused by the track to the number of straw hits contained in the clusters associated to that track. In the case of double-hit clusters, two hits are counted if both hits come from the correct VELO track and zero otherwise. The distributions for tracks passing all straw-tube planes, i.e. where 8 straw hits are expected, are shown in Fig. 10. Only a small loss in the efficiency for finding correct hits as a result of the clusterization procedure is observed. The slightly reduced mean number of hits per track (6.6 instead of 7.1) after the clusterization procedure does not lead to a significant inefficiency in the TT1 reconstruction performance.

The resolution for double-hit straw clusters is shown in Fig. 11. The obtained value of 320 μm is in agreement with the naive expectation of 400 $\mu\text{m}/\sqrt{2} \approx 280$ μm.

3.3 Baseline algorithm

In both the silicon and the straw-tube case, the clusterization procedure leaves us with a set of space points, which are treated in exactly the same way for both cases and which, for simplicity, we shall call "hits" again in the following. The TT1 matching algorithm looks for such hits within a geometrical search window defined by the extrapolation of the VELO track to be matched. Since only high-momentum tracks are relevant for the application in the Level-1 trigger, the track search in TT1 is restricted to tracks with momentum above 3 GeV. This corresponds to a deflection distance of about ± 15 mm with respect to the (straight) VELO track extrapolation at TT1 for the magnetic field map used. For a given VELO track, a histogram in a plane close to the TT1 detector, centred around the intersection of that plane with the VELO track extrapolation, with a width of ± 15 mm and a bin size of 1 mm is constructed (see Fig. 12). For each TT1 hit the distance

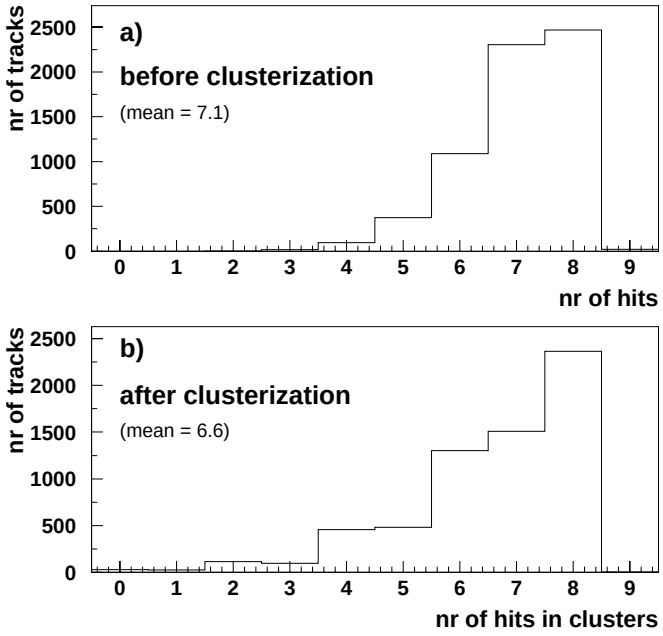

Figure 10: The distribution of the number of correct hits on a track a) before and b) after the straw-tube clusterization procedure (see text).

in projection between the hit and the straight VELO track extrapolation line is calculated and filled into the histogram. Once the histogram is filled, a search for accumulations in the histogram is performed, starting from the centre of the histogram going outwards. A track traversing and leaving hits in all four TT1 layers is expected to give an accumulation of four entries. Accumulations are considered as track candidates if they contain at least three entries in five consecutive bins. This window (5 mm) is significantly larger than the expected spread due to the detector resolution to account for multiple scattering effects. The reconstruction performance does not depend on the exact method applied for the search for accumulations in the histogram, as was checked by varying the bin size and changing the definition of an accumulation within reasonable limits.

For each accumulation found, the following iterative track reconstruction procedure is applied: The magnetic field in the TT1 area being relatively weak, we can use a simple line fit to the hit coordinates with fixed x- and y-slopes:

$$x = s_x z + x_0$$
$$y = s_y z + y_0$$

where x_0, y_0 are free parameters of the fit defined as the offsets at $z = z_0$, defined to be at the centre of TT1. The slopes s_x and s_y in x and y, respectively, are fixed in the fit and given by the line connecting the last measured VELO point and the point

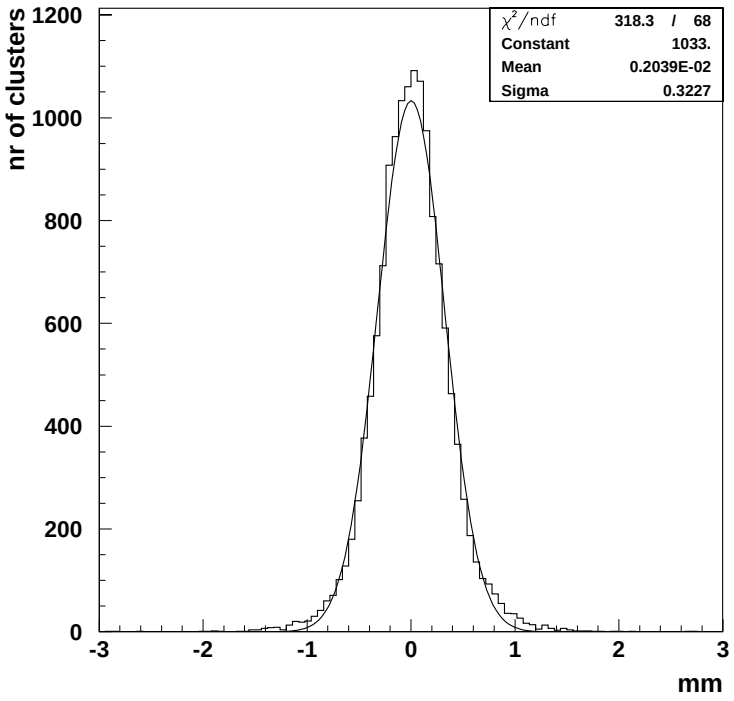

Figure 11: The resolution of double hit straw-tube clusters.

(x_0,y_0,z_0) as obtained from the previous iteration. In the case of the x-slope, a small correction $k\alpha$ is added where α is the angle between the line described above and the extrapolation line of the VELO track, and k is an empirically determined constant factor (found to be ≈2.35 for a detector geometry with vertical RICH design). The χ^2 of the fit is computed and the hit with the highest χ^2 contribution is removed if the total χ^2 is larger than a certain maximum value $\chi^2_{\rm max}$ (nominally $\chi^2_{\rm max} = 9$). The x- and y-slopes are adjusted after each iteration. The track candidate is accepted if this iteration stops with at least three hits left and if the final χ^2 is less than $\chi^2_{\rm max}$. Otherwise the algorithm moves on outwards in the histogram to the next accumulation and so on until either a successful match has been found or all accumulations have been examined without success.

For an accepted track candidate (combination of hits) the momentum is determined as a function of the deflections in the two halves of TT1, Δx_1 and Δx_2, the slopes of the associated VELO track, $s_x^{\rm VELO}$ and $s_y^{\rm VELO}$, as well as the mean value $z^{\rm TT1}$ of the z coordinates of all TT1 hits forming the candidate:

$$1/p = F(\Delta x_1, \Delta x_2, s_x^{\rm VELO}, s_y^{\rm VELO}, z^{\rm TT1})$$

The function F, parametrized as a second-order polynomial in its arguments, is determined exclusively by the magnetic field map. The average momentum resolution

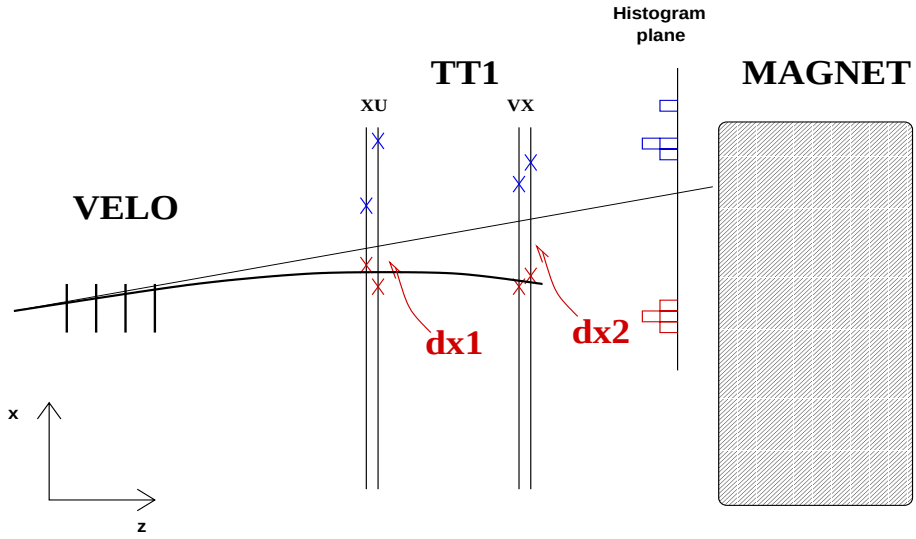

Figure 12: Illustration of the TT1 reconstruction procedure.

of the procedure is measured to be 26% for properly reconstructed tracks in TT1 with momentum above 3 GeV. The dependence of the resolution with the momentum and the technology choice for the TT1 tracking station are shown in Fig. 13 and Fig. 14.

Knowing the momentum of the track, an error estimate for the displacement in y can be obtained as the quadratic sum of two components:

$$\sigma_y(p) = \sqrt{(\sigma_y^{\rm det})^2 + (\sigma_y^{\rm MS}(p))^2} \quad ,$$

with $\sigma_y^{\rm det}$ depending only on the VELO and TT1 resolutions and the momentum-dependent $\sigma_y^{\rm MS}(p)$ determined according to the expected scattering in the detector material. We then reject track candidates with $\Delta y > 4\sigma_y$. Finally, we require that track candidates have at least one hit in each half of TT1, and at least one hit each in the stereo and x layers of the detector.

3.4 Performance with regard to trigger application

The performance of the TT1 matching algorithm was evaluated with regard to the two characteristics crucial for the trigger application, signal efficiency and retention of minimum-bias events. To study the effect on signal efficiency, we look at the reconstruction efficiency for tracks with true momentum larger than 5 GeV (Sec. 3.4.1). To assess the probability of random triggers due to wrong p_T assignements we analyze the source of tracks that give a reconstructed p_T of more than 1 GeV, i.e. determine the fractions of correctly and wrongly matched tracks in this sample (Sec. 3.4.2).

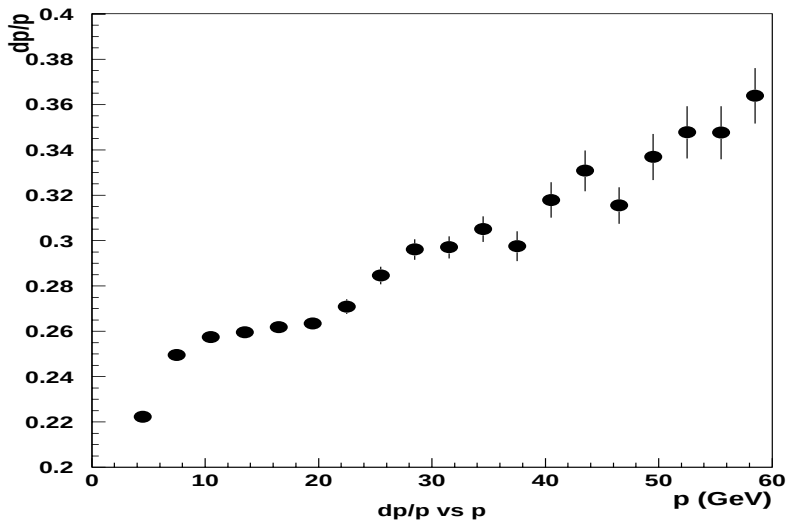

Figure 13: The relative momentum resolution of properly reconstructed tracks in the full-Si TT1 as a function of the momentum.

3.4.1 Reconstruction efficiency for tracks with momentum above 5 GeV

The performance study of the TT1 matching algorithm proceeds in a several steps. First the reconstruction procedure is checked in a clean environment without applying the requirements on $\chi^2_{\max}$ and Δy and using only correct (Monte-Carlo truth checked) TT1 hits. For this case we define an efficiency

$$\varepsilon_0 = N_0/N_{\text{all}}$$

where N_0 indicates the number of reconstructed tracks from the reference track sample of N_{all}. Tracks in the reference sample are tracks with more than 5 GeV (true) momentum that fulfil the selection criteria of the TT1 reconstruction on the basis of their true hits, i.e. they should have at least three TT1 hits in total, among those at least one stereo and one x hit and at least one hit in each of the two halves of TT1. Since a 5 GeV track should have all hits inside the histogram used for the reconstruction, this efficiency is expected to be close to 100%. The results are very similar for the silicon and the straw tube technology, where in both cases we only consider the outer part of the detector (Outer Tracker area). An efficiency of $\varepsilon_0 \approx 98\%$ is measured in both cases. The small inefficiency of 2% was found to be the result of either some of the hits being outside the search window or of a wider spread of the hits in the histogram than required (i.e. less than three hits in five consecutive bins). A possible reason for this are the elastic but hard scatterings generated during the GEANT particle transport through the detector material. The result for ε_0 demonstrates that the reconstruction algorithm is highly efficient for tracks satisfying the reconstruction criteria at the Monte Carlo truth level, for both the silicon and the straw technology.

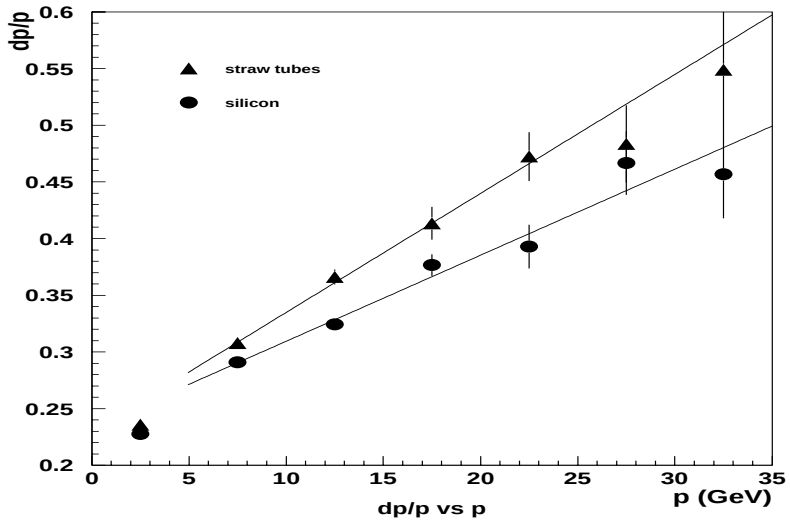

Figure 14: The relative momentum resolution of properly reconstructed tracks in the outer region of TT1 as a function of the momentum and technology choice.

In the next step the same efficiency, now called ε_1, is measured after applying nominal cuts at $\chi^2 < \chi^2_{\max} = 9$ and $\Delta y < 4\sigma_y$ but still allowing only correct hits to enter the histogram. The results of this exercise are presented in Table 3.4.1. The overall efficiencies are similar. Only a small difference can be seen in the rates of tracks rejected by the χ^2 and Δy criteria arising from the different detector resolutions.

Finally the efficiencies ε_2 for nominal conditions were estimated by collecting all hits inside the search window. At this point one can measure the rate of correct and wrong TT1 matchings. Track candidates containing at least two correct TT1 hits are counted as correct matches, all others are considered wrong matches. The results are shown in Table 3.4.1. Now we can observe a slight difference in the overall track efficiencies. The efficiency for the silicon technology drops from 84% to 78% while the efficiency of the straw tubes remains the same. However in the case of the straw detector only 93% of the reconstructed tracks are correct matches. This eventually leads to the same total efficiency of correct matchings shown in the last row of the table. Therefore, for tracks above 5 GeV momentum, the performance of the TT1 track reconstruction is comparable for the silicon and the straw technology.

3.4.2 The composition of the sample of reconstructed tracks

In the previous section the reconstruction efficiency for tracks with true momentum above 5 GeV was considered to compare the performance of the TT1 reconstruction for tracks coming from the signal channels. In this case, a possible contamination of false trigger tracks does not significantly increase the signal efficiency since

Table 2: Efficiencies ε_1 after requiring $\chi^2 < 9$ and $\Delta y < 4\sigma_y$ and using only correct hits. Also shown are the corresponding rates of lost events from various sources. For both technologies, the numbers are given for the outer part of TT1 only (Outer Tracker area).

	straw	silicon
efficiency ε_1	84%	84%
inefficiencies due to:		
no hit	2%	2%
χ^2 cut	10%	5%
Δy cut	4%	9%

Table 3: Track-matching efficiencies ε_2 after requiring $\chi^2 < 9$ and $\Delta y < 4\sigma_y$ and using all TT1 hits. The rate of correct matchings is normalized to *all* matched tracks. The last row gives the product of the efficiency ε_2 and the rate of correct matchings, i.e. the total efficiency to match correctly TT1 hits to a VELO track with momentum higher than 5 GeV. For both technologies, the numbers are given for the outer part of TT1 only (Outer Tracker area).

	straw	silicon
efficiency ε_2	84%	78%
correct matchings	93%	99.7%
efficiency for correct matching	78%	78%

Table 4: The relative rates of correct and wrong matchings to tracks with reconstructed transverse momentum larger than 1 GeV. Also shown is the rate for matchings to VELO ghost tracks. For both technologies, the numbers are given for the outer part of TT1 only (Outer Tracker area).

matching	straw	silicon
correct	77%	98%
wrong	13%	1%
to VELO ghost	10%	1%

the B tracks typically already satisfy the trigger condition. A completely different, but just as important aspect of the trigger performance is the capability of rejecting minimum-bias events. Here, the number of triggering tracks is small and any momentum misassignement can lead to a significant increase in accepted minimum-bias events. Thus the performance strongly depends on the rate of wrongly assigned tracks in the TT1 matching procedure. To study this effect we compare the reconstructed and true transverse momenta on the sample of all reconstructed tracks. In Table 3.4.2 the composition of the tracks with reconstructed transverse momentum exceeding 1 GeV is shown. A significant difference in reconstruction purity between the straw and the silicon technology is observed. In the straw-tube case, a large fraction (23%) of tracks is assigned an incorrect momentum due to either wrong matchings to good VELO tracks or associations to VELO ghost tracks.

This difference in the purity of the matching is presented graphically in Fig 15. The distribution of true transverse momentum $p_T^{\rm true}$ is shown for tracks where the reconstructed transverse momentum $p_T^{\rm rec}$ is 50% larger than $p_T^{\rm true}$. Matchings to VELO ghost tracks are included in the first bin. One can see that the source of the difference is in the range of low $p_T^{\rm true}$. In the case of the straw-tube technology, a significant number of low-p_T tracks are reconstructed as high-p_T tracks. For the same area in silicon the situation is much cleaner.

Another illustration of the same effect is given in Fig.16 where the true transverse momentum is plotted versus the reconstructed one for tracks with $p_T^{\rm rec} > 1$ GeV. The band of wrong associations can clearly be seen at low $p_T^{\rm true}$. There are two main sources of this difference: the detector resolution and the detector segmentation along y (straws are longer than silicon strips, see Sec. 3.1). Fig 17 shows why, in spite of the same track density the number of wrong matchings is higher for the straw tubes than for silicon strips in the same area of TT1. The larger errors assigned to the same combination of accidental hits in the case of the straw-tube detector leads to the acceptance of the combination whereas the smaller errors in the silicon case result in a rejection. If such a combination of hits comes from a real particle accidentally traversing TT1 close to the VELO extrapolation, the better y resolution in the silicon case gives an enhanced rejection power because of the higher sensitivity to the x and y slopes. In addition, the lack of segmentation in the y coordinate in

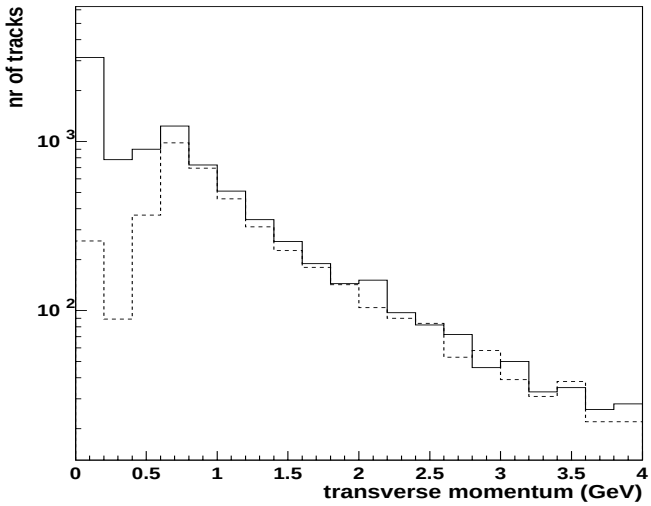

Figure 15: The distribution of $p_T^{\rm true}$ for the straw-tube (solid line) and the silicon technology (dashed line), for tracks with $p_T^{\rm rec} > 1$ GeV and $p_T^{\rm rec} > 1.5 \times p_T^{\rm true}$. Only TT1 tracks in the outer part of TT1 (Outer Tracker area) are shown.

the case of the straw tubes results in an increased number of accidental combinations of hits and therefore more wrong matchings (see also Sec. 4.5.3).

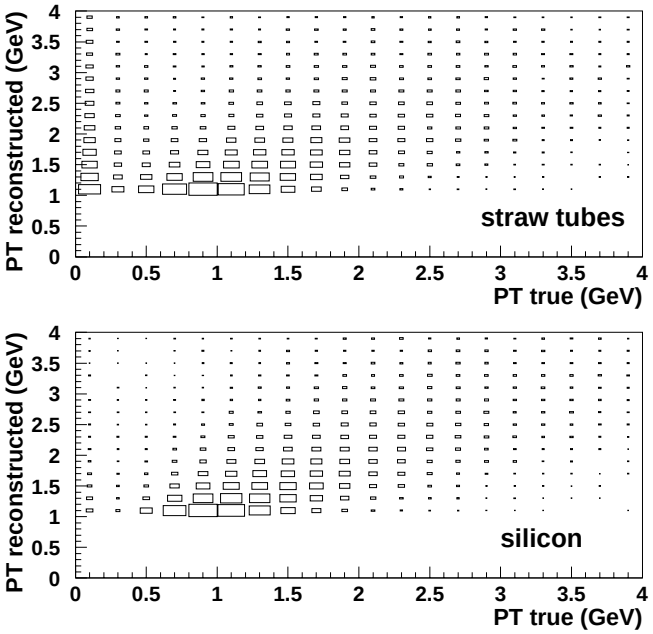

Figure 16: The distributions of true transverse momentum versus the reconstructed one for the outer part of TT1 for the straw-tube and the silicon option.

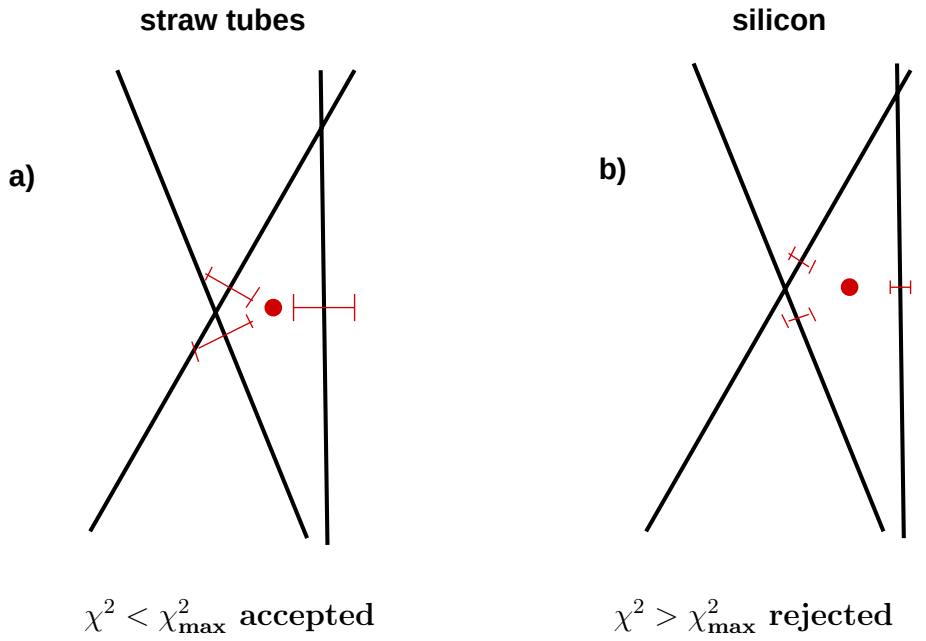

Figure 17: Schematic illustration of the difference in the treatment of random combination of close hits in the TT1 reconstruction algorithm for two different detector resolutions.

4 The mini-Level-1 algorithm and its performance

4.1 Trigger strategy

The principal idea of mini-Level-1 is to combine the two most characteristic properties of b tracks available at this early trigger stage, impact parameter and transverse momentum, to form an efficient selection of events containing b-hadrons. The trigger strategy must also account for the fact that the determination of the transverse momentum is expensive and should therefore be limited as far as possible to tracks that are otherwise likely to be b tracks. Therefore, the extrapolation to TT1 for obtaining a p_T estimate is only performed on a subset of tracks, preselected to be within a certain range of impact parameter. We currently apply a lower limit of 100 μm and an upper limit of 3 mm in impact parameter (the latter limit motivated by the rejection of K_S tracks), and require that an event contain at least two tracks within these limits.

Studies based on Monte Carlo truth information have shown that for a two-body decay of the b hadron (for instance $B^0_d \to \pi^+\pi^-$), a minimum requirement on the highest p_T present in this set of tracks already results in an almost optimal trigger performance (in the sense that we were unable to find a better-performing algorithm). However, for higher-multiplicity decays of the b-hadron, it turns out to be more advantageous to base the trigger decision on the *two highest-p_T tracks.* This results in a stronger involvement of the tracks from the accompanying b hadron, which helps select signal B decays with relatively weak signature while still efficiently rejecting minimum-bias events.

4.2 Discriminant variables

In the current version of the mini-Level-1 algorithm, we use four variables to construct a suitable trigger variable on which to perform the selection. The four variables are computed from those two tracks which have the highest p_T, as determined via extrapolation to TT1, among the preselected tracks (impact parameter d between 100 μm and 3 mm). If no p_T estimate can be obtained for a track, a value of $p_T = 400$ MeV (the average p_T for VELO tracks) is assigned to it. After this assignement the track is treated as if it had a measured p_T and can still contribute to the trigger decision. The four variables used for the trigger decision are then:

PT1 – The transverse momentum (p_T) of the first track.

PT2 – The transverse momentum of the second track.

IPS1 – The impact parameter significance (d/σ_d) of the first track.

IPS2 – The impact parameter significance of the second track.

Figs. 18 and 19 show the distribution of these variables (and two linear combinations) for minimum-bias events, signal events, and signal events within geometrical and kinematic acceptance (see following section) in direct comparison. Also shown are

the corresponding purities defined as the ratio of (useful) signal events to minimum-bias events for a particular bin of the variable in question.

4.3 Normalization of signal event samples

The overall aim of the trigger is the maximization of the final sample of reconstructed signal events. Therefore it should be optimized for the highest efficiency for events that indeed can be reconstructed. However, it is not straightforward to define "reconstructibility". An undisputed criterion, at least for exclusively reconstructed channels, is that all daughter tracks must have hits in the detector acceptance. We enforce this by requiring at least one hit in the VELO as well as in each of the seeding stations ST1 to ST3 for all daughter tracks of a signal B meson.

On top of the purely *geometrical* acceptance there may be important *kinematic*, *reconstruction* and *flavour tagging* selection biases. They depend on the specific analysis applied, and may well change with time and understanding of the detector. To obtain an approximation to a typical offline selection, we decided to adopt the momentum requirements applied for the physics studies performed for the Technical Proposal, and to apply them at the Monte-Carlo truth level.

All signal tracks must have a total momentum in the range between 1 and 100 GeV/c given by the pion-kaon separation limit of the RICH detector. Below we list the additional momentum requirements specific to the three decay channels considered for the performance study (Sec. 4.5):

- $\mathrm{B_d^0} \to \pi^+\pi^-$
  - $p_T > 1$ GeV/c for both pions;
  - $p_T > 3.5$ GeV/c for at least one pion;
  - $p_T > 3$ GeV/c for the $\mathrm{B_d^0}$.
- $\mathrm{B_s^0} \to \mathrm{D_s^-}(\mathrm{K^+K^-}\pi^-)\mathrm{K^+}$
  - $p > 2$ GeV/c for all daughter tracks;
  - $p > 3$ GeV/c for the direct (bachelor) kaon;
  - $p_T > 2$ GeV/c for the $\mathrm{D_s^-}$.
- $\mathrm{B_d^0} \to \overline{\mathrm{D}}^0(\mathrm{K^+}\pi^-)\mathrm{K^{*0}}(\mathrm{K^+}\pi^-)$
  - no channel-specific requirements

Since the requirements on the track momenta are of a somewhat subjective nature, we will quote trigger performance numbers for both cases, i.e., for signal samples that merely fulfil the acceptance condition as well as for those that satisfy the kinematic requirements.

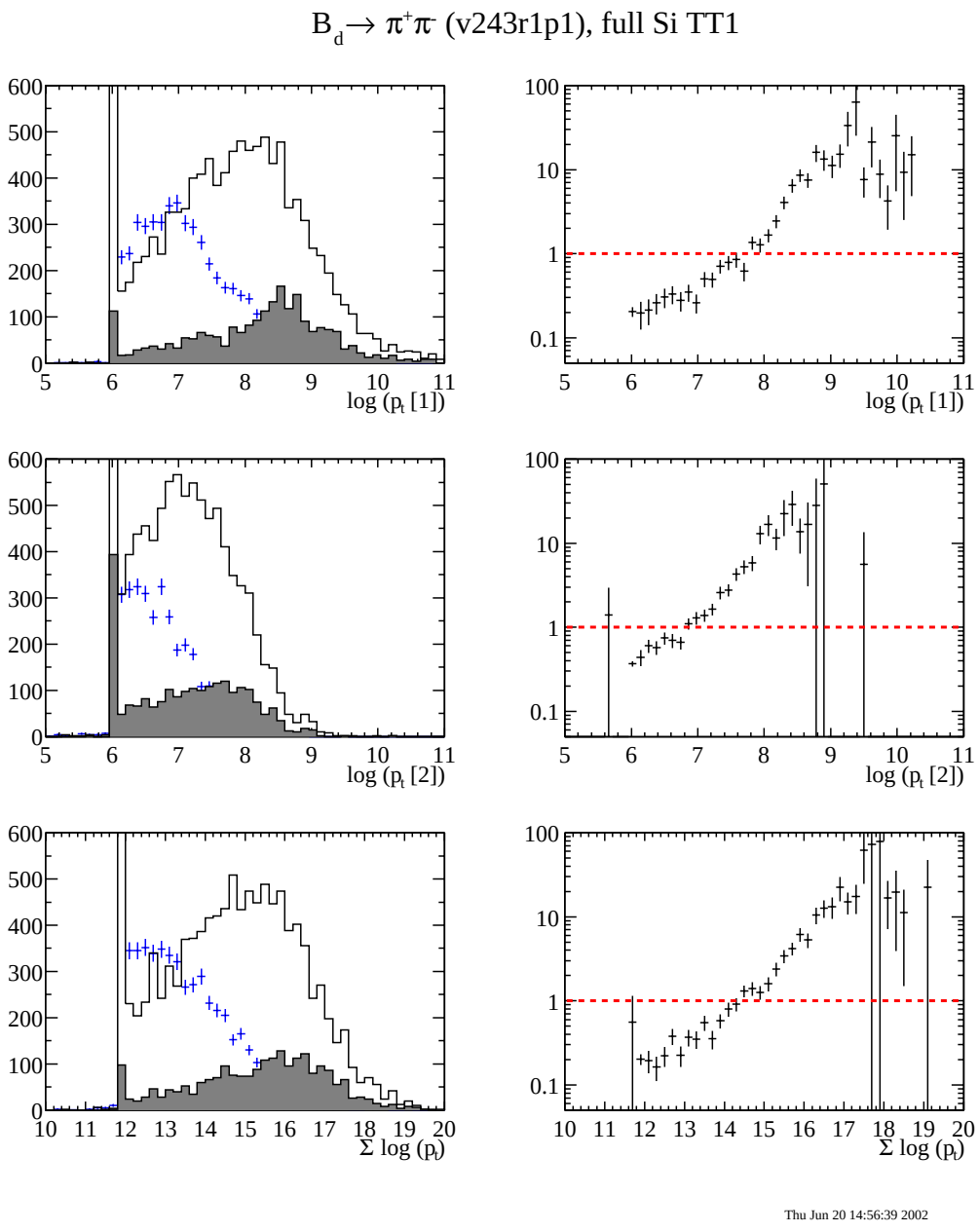

Figure 18: Left: Distributions of the transverse momenta for the two trigger tracks (PT1 and PT2, logarithmic scale) for minimum-bias events (error bars), signal events (white histograms) and signal events in the detector acceptance with typical offline kinematic requirements applied at the Monte-Carlo truth level (hatched histograms). The third plot shows these distributions for the sum log(PT1)+log(PT2). Right: Purity plots for the same variables (see text).

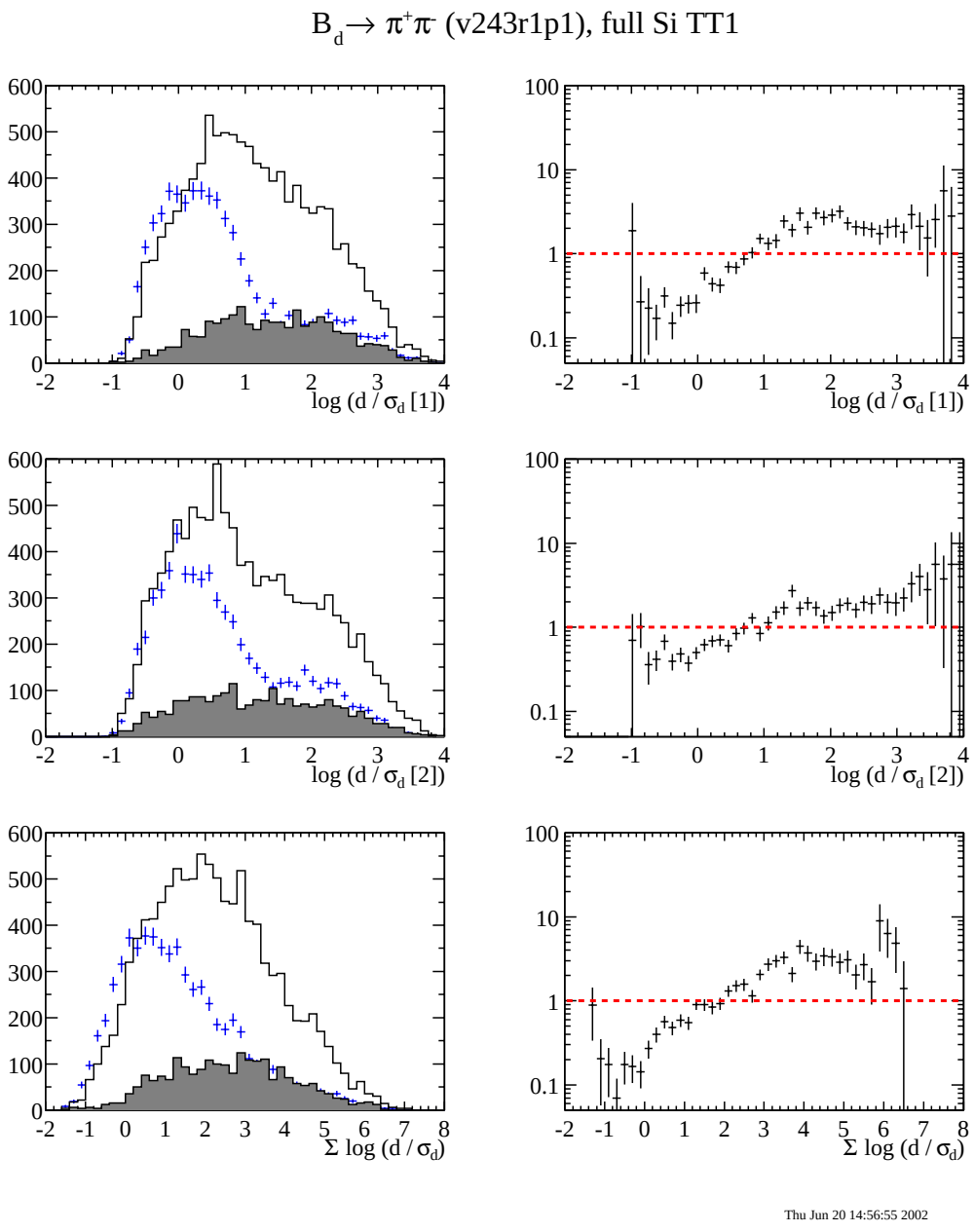

Figure 19: Left: Distributions of the impact parameter significances for the two trigger tracks (IPS1 and IPS2, logarithmic scale) for minimum-bias events (error bars), signal events (white histograms) and signal events in the detector acceptance with typical offline kinematic requirements applied at the Monte-Carlo truth level (hatched histograms). The third plot shows these distributions for the sum log(IPS1)+log(IPS2). Right: Purity plots for the same variables (see text).

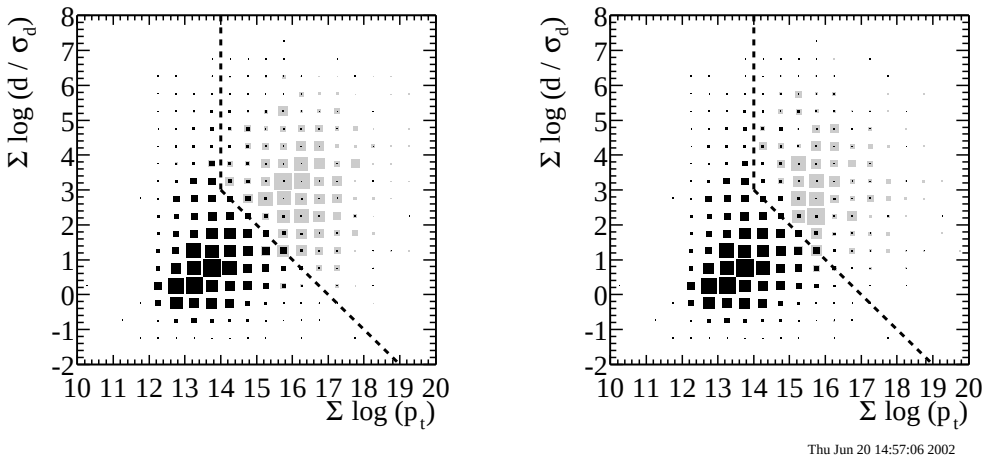

Figure 20: Distribution of minimum-bias events (black) and signal events in the detector acceptance with typical offline kinematic requirements applied at the Monte-Carlo truth level (grey) in the plane of the two variables log(PT1)+log(PT2) versus log(IPS1)+log(IPS2). Left for $B^0_d \to \pi^+\pi^-$, right for $B^0_s \to D^-_s(K^+K^-\pi^-)K^+$. The dashed line represents the vertical-diagonal cut applied for the mini-Level-1 selection.

4.4 Definition of the trigger variable

Several possibilities to combine the four discriminating variables into one trigger variable have been studied, such as an optimized linear combination (Fisher discriminant) or non-linear cuts in higher dimensions. The best performance for all channels considered, without resorting to overly complicated and fine-tuned strategies, was achieved by a simple two-dimensional cut in the variables log(PT1)+log(PT2) and log(IPS1)+log(IPS2). Fig. 20 shows the disribution of minimum bias events and two types of signal events in these two variables, and the vertical-diagonal cut that is used to define the trigger variable. We define the trigger variable as the normal two-dimensional distance of an event to the cut line. The trigger performance is found to be rather stable against moving the position of the "kink" of the cut by 1–2 units in each direction.

The trigger definition outlined here serves as a first optimized version of the mini-Level-1 algorithm suitable for the performance studies needed for finalizing the LHCb-light design. It may of course change with new tracking algorithms and ideas becoming available.

4.5 Performance of the mini-Level-1 algorithm

To demonstrate the performance of the mini-Level1 algorithm we select three decay channels which differ in their numbers of primary daughter tracks (likely to have high p_T): $B^0_d \to \pi^+\pi^-$ with two, $B^0_s \to D^-_s(K^+K^-\pi^-)K^+$ with one, and $B^0_d \to \overline{D}^0(K^+\pi^-)$ $K^{*0}(K^+\pi^-)$ with no primary daughters.

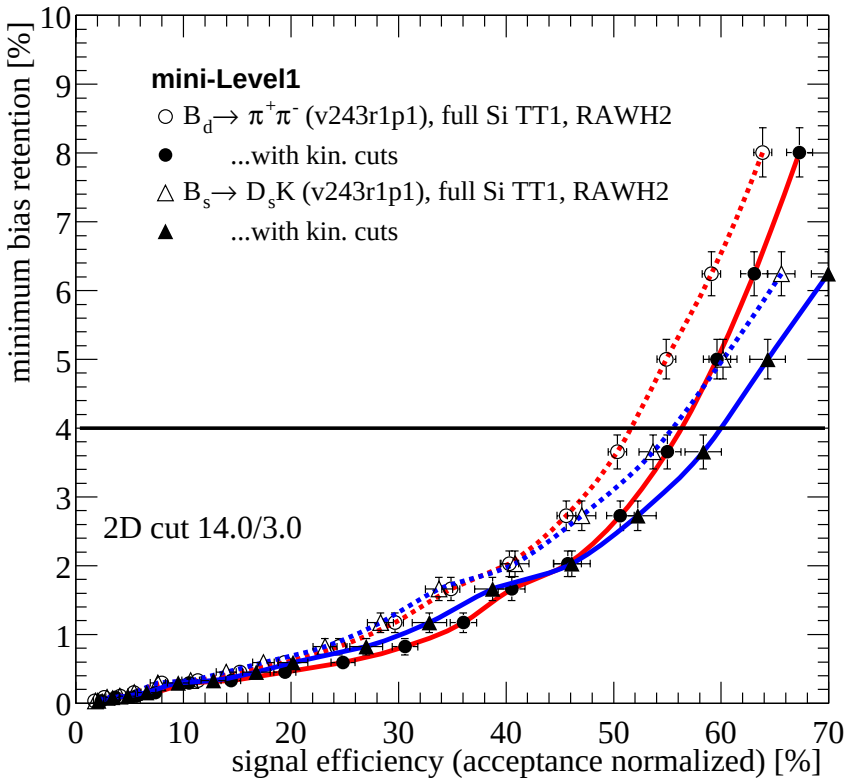

Figure 21: Signal efficiency versus minimum-bias retention rate for varying mini-Level-1 cut for full-silicon TT1. The efficiencies are normalized to events that are in the geometrical acceptance and fulfil a set of typical offline kinematic requirements, applied at the Monte-Carlo truth level. Simulated data with pile-up for a luminosity of $\mathcal{L} = 2 \times 10^{32}$ cm^{-2}s^{-1}.

4.5.1 Performance for the full-silicon TT1

In Fig. 21 we show the minimum bias retention versus the signal efficiency. The full-silicon option for TT1 (database v243r1p1) was used to obtain this figure. Simulated data contains pile-up for a nominal LHCb luminosity of $\mathcal{L} = 2 \times 10^{32}$ cm^{-2}s^{-1}. Only two signal channels are shown as the channel $B_d^0 \rightarrow \overline{D}^0 K^{*0}$ was not available for these conditions.

It should be noted that the signal efficiencies cannot be compared to efficiencies on offline selected samples. Our normalization sample is the result of acceptance and some kinematic requirements only; a true offline selection will also require high impact parameters (long lifetimes) eliminating a large part of the events not triggered by mini-Level-1, thereby boosting considerably the relative trigger efficiency.

4.5.2 Comparison between TT1 implementations

In Figs. 22 (efficiencies) and Fig. 23 (efficiency versus retention) we compare the performance of the mini-Level-1 algorithm for the two TT1 implementations, full-silicon and mixed silicon-straw design at high luminosity ($\mathcal{L} = 5 \times 10^{32}$ cm^{-2}s^{-1}). Also shown, for illustration, is the (hypothetical) case where no information from the Outer-Tracker area of TT1 would be used in the trigger. Table 5 summarizes all the efficiencies and retention rates obtained from this simulation study. We list the total numbers of Level-0 and Level-1 triggers as well as the numbers of triggered events that are in the acceptance and that fulfil the kinematic requirements described above.

The comparison shows that the full-silicon TT1 option improves the trigger efficiency by 22–26% for the channels $B_d^0 \to \pi^+\pi^-$ and $B_d^0 \to \overline{D}^0 K^{*0}$, and even 42% (52% with kinematic selection) in the case of $B_s^0 \to D_s^- K^+$. Keeping the signal efficiencies constant, the retention-versus-efficiency curves indicate that with the full-silicon option, the retention of minimum-bias events is lower by a factor of about two.

4.5.3 Dependence on detector resolution and other effects

Since the assumed online-achievable resolution of 400 μm for the straw-tube part of the mixed-technology TT1 is obtained "by hand" via smearing in the digitisation process, it is straight-forward to study the effect of this resolution on the final trigger performance.

In Fig. 24 we show the obtained efficiency curves for the channel $B_d^0 \to \pi^+\pi^-$ as well as the retention of minimum-bias events assuming resolutions of 200, 400 and 800 μm for the straw tubes. The curves for full-silicon TT1 and no trigger information from the outer part of TT1 are also shown for comparison. Clearly, worse resolution in the straw tubes increases the minimum-bias retention rate considerably and therefore deteriorates the overall trigger performance. This effect is however compensated to some degree by an increase in signal efficiency caused by more random accepts, such that the effect on the overall trigger performance is not quite as large (Fig. 25).

Similar studies have been performed using simulated data for the full silicon setup, but assuming worse resolution for the silicon hits in the Outer Tracker area and mimicking the y-segmentation of the straw tubes when performing the track reconstruction. The result of all these studies is that the superior hit resolution of the silicon detector is the main cause of the better performance of the full-silicon design of TT1 in the trigger as compared to the mixed solution. The finer segmentation in y also plays a role, particularly for worse hit resolutions. But even when assuming equal resolutions and y-segmentations in the Outer Tracker area, the full-silicon design still performs somewhat better thanks to the absence of any left-right ambiguities and due to differences in the layout of the detector planes (see Sec. 3.1).

Although detector resolution is the dominant effect in this comparison, the detector geometry and segmentation are affecting the trigger performance and therefore must be important considerations for the final design of this tracking station, whichever technology is chosen. They are however beyond the scope of this note.

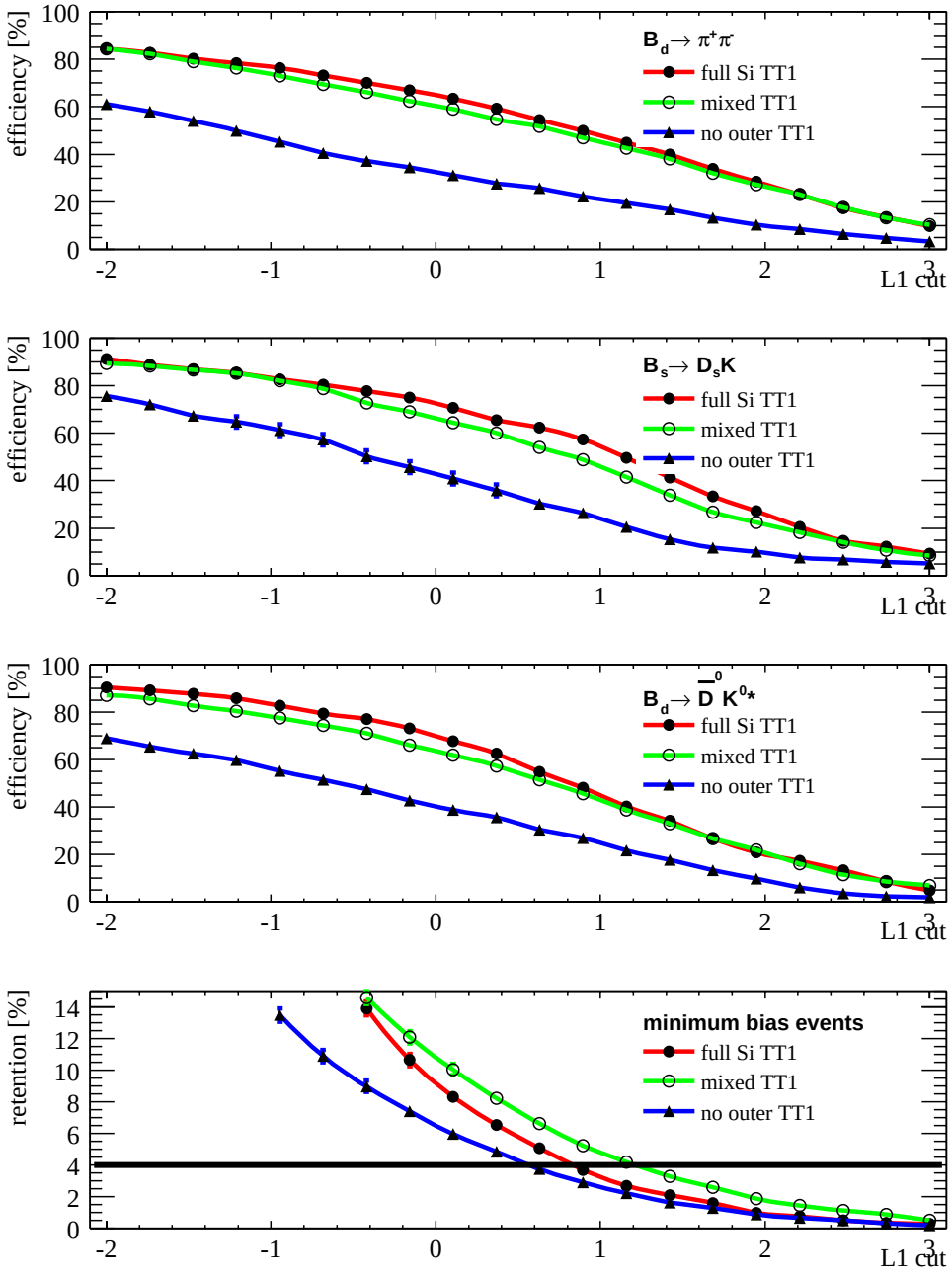

Figure 22: Signal efficiency and minimum-bias retention rate as a function of the mini-Level-1 cut, comparison between three different TT1 implementations: full silicon, mixed silicon-straw, and, for illustration, no read-out of the Outer-Tracker area. The signal efficiencies are shown for signal events that are in the geometrical acceptance *and* fulfil a set of typical offline kinematic requirements, applied at the Monte-Carlo truth level. Simulated data with pile-up for a luminosity of $\mathcal{L} = 5 \times 10^{32}$ cm^{-2}s^{-1}.

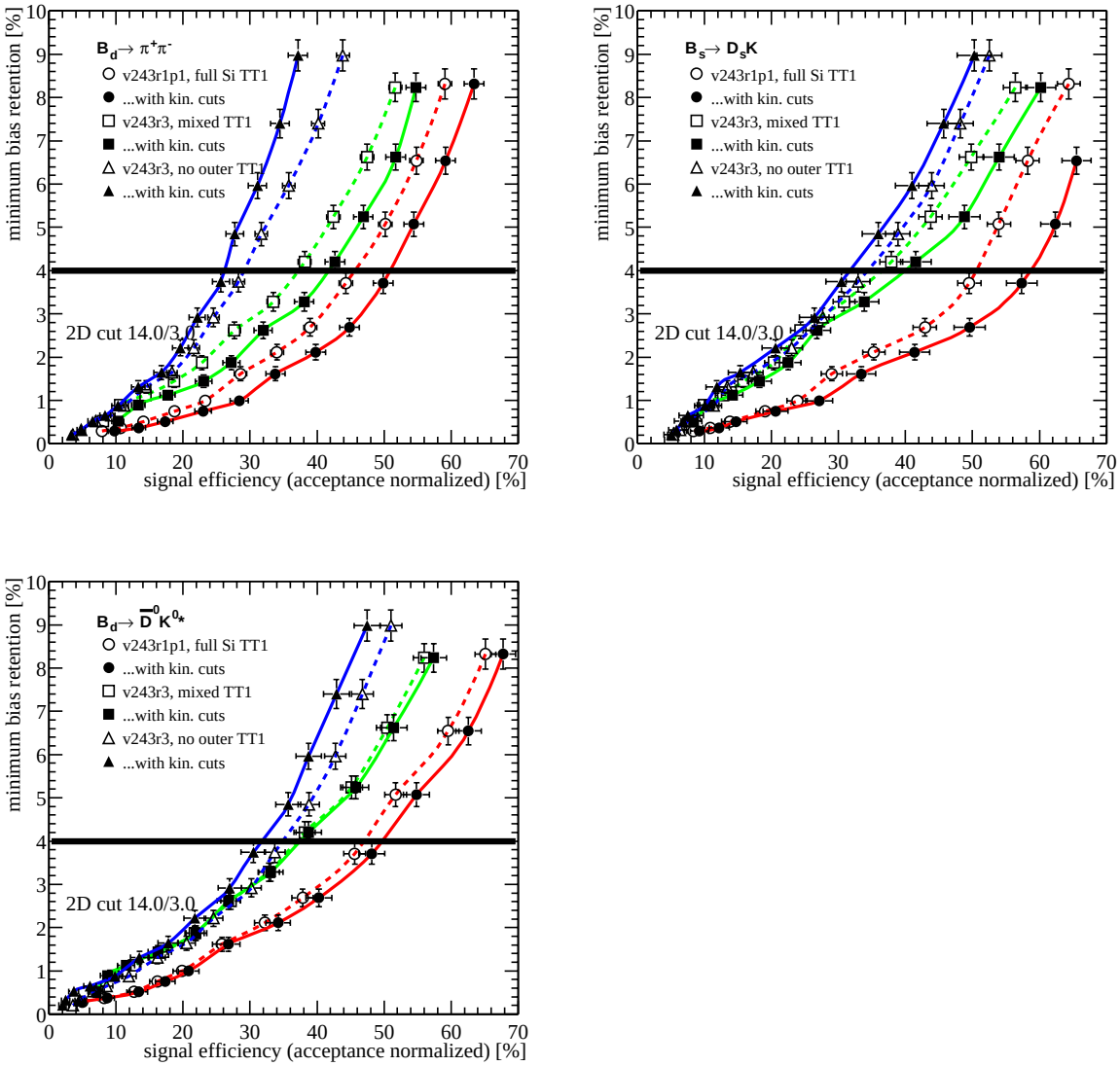

Figure 23: Signal efficiency versus minimum-bias retention rate for varying mini-Level-1 cut. The signal efficiencies are plotted for signal events that are in the geometrical acceptance (open symbols and dashed lines) as well as for signal events that fulfil a set of typical offline kinematic requirements, applied at the Monte-Carlo truth level (full symbols and solid lines). Each plot compares, for one decay channel, the mini-Level-1 performance for three different TT1 implementations: full silicon, mixed silicon-straw, and, for illustration, no read-out of the Outer-Tracker area. Upper left: $B_d^0 \to \pi^+\pi^-$, upper right: $B_s^0 \to D_s^-(K^+K^-\pi^-)K^+$, and lower left $B_d^0 \to \overline{D}^0(K^+\pi^-)K^{*0}(K^+\pi^-)$. Simulated data with pile-up for a luminosity of $\mathcal{L} = 5 \times 10^{32}$ cm^{-2}s^{-1}.

Table 5: Summary of the simulation study of the mini-Level-1 performance for various implementations of TT1.

TT1 technology	Decay channel	Evts. proc.	L0 trigs.	L0 trigs. in acc.	L0 trigs. kin. cuts	L1 trigs.	L1 trigs. in acc.	L1 trigs. kin. cuts
full Si TT1	$B_d^0 \to \pi^+\pi^-$	20k	5471 (27.4%)	2492	1113	1746	1104 (44.3%)	556 (50.0%)
(v243r1p1)	$B_s^0 \to D_s^- K^+$	15500	3872 (25.0%)	814	476	1190	400 (49.1%)	274 (57.6%)
RAWH3	$B_d^0 \to \overline{D}^0 K^{*0}$	19999	4890 (24.5%)	938	658	1491	424 (45.2%)	315 (47.9%)
	minimum bias	90k	6251 (6.95%)	–	–	250	–	–
Si/Straw TT1	$B_d^0 \to \pi^+\pi^-$	20k	5495 (27.5%)	2566	1158	1404	928 (36.2%)	473 (40.8%)
(v243r3)	$B_s^0 \to D_s^- K^+$	15806	3922 (24.8%)	805	467	914	278 (34.5%)	177 (37.9%)
RAWH3	$B_d^0 \to \overline{D}^0 K^{*0}$	20k	4868 (24.3%)	941	653	1153	348 (37.0%)	249 (38.1%)
	minimum bias	99599	6947 (6.97%)	–	–	252	–	–
no outer TT1	$B_d^0 \to \pi^+\pi^-$	20k	5495 (27.5%)	2566	1158	1157	733 (28.6%)	297 (25.6%)
(v243r3)	$B_s^0 \to D_s^- K^+$	13806	3442 (24.9%)	695	398	721	237 (34.1%)	128 (32.2%)
RAWH3	$B_d^0 \to \overline{D}^0 K^{*0}$	20k	4868 (24.3%)	941	653	1046	326 (34.6%)	208 (31.9%)
	minimum bias	89599	6271 (7.0%)	–	–	250	–	–
full Si TT1	$B_d^0 \to \pi^+\pi^-$	20k	7150 (35.8%)	3313	1513	2610	1700 (51.3%)	843 (55.7%)
(v243r1p1)	$B_s^0 \to D_s^- K^+$	20k	6268 (31.3%)	1416	852	2290	780 (55.1%)	505 (59.3%)
RAWH2	minimum bias	91500	5718 (6.25%)	–	–	229	–	–

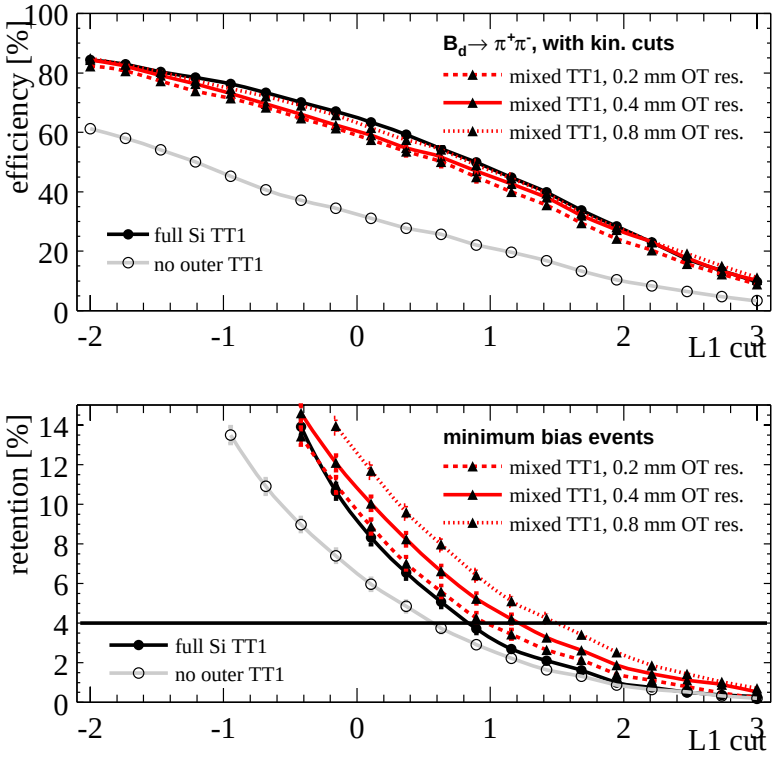

Figure 24: Signal efficiency ($B^0_d \rightarrow \pi^+\pi^-$) and minimum-bias retention rate as a function of the mini-Level-1 cut, comparison between different resolutions for the straw-tube part of a mixed-technology TT1. The curves for full-silicon TT1 and no trigger information from the outer part of TT1 are also shown for comparison. The efficiencies are normalized to events that are in the geometrical acceptance and fulfil a set of typical offline kinematic requirements, applied at the Monte-Carlo truth level. Simulated data with pile-up for a luminosity of $\mathcal{L} = 5 \times 10^{32}$ cm^{-2}s^{-1}.

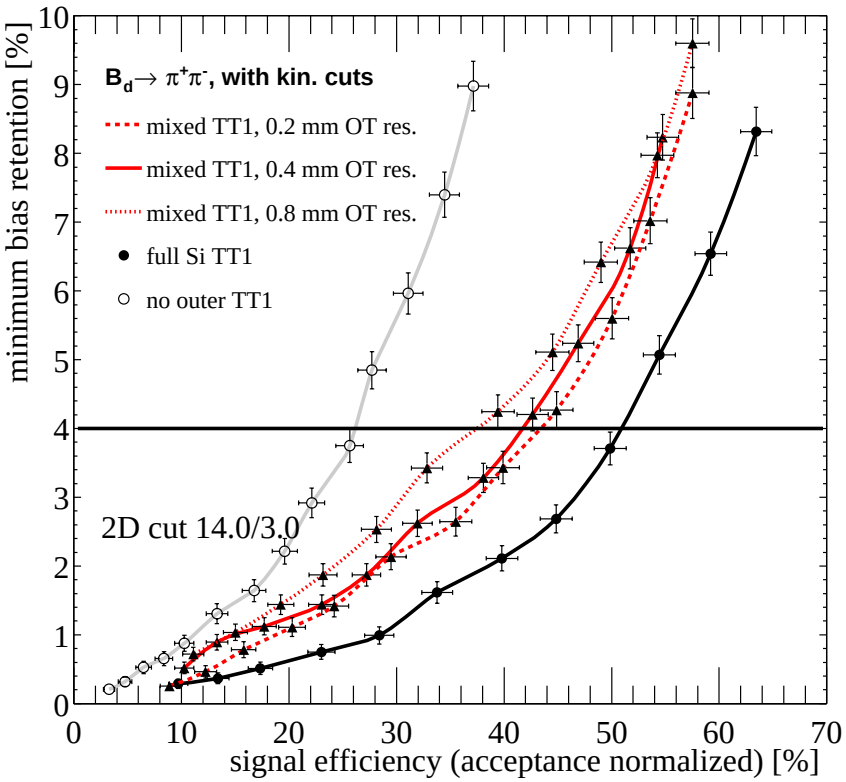

Figure 25: Signal efficiency ($B^0_d \rightarrow \pi^+\pi^-$) versus minimum-bias retention rate for varying mini-Level-1 cut, comparison between different resolutions for the straw-tube part of a mixed-technology TT1. The curves for full-silicon TT1 and no trigger information from the outer part of TT1 are also shown for comparison. The efficiencies are normalized to events that are in the geometrical acceptance and fulfil a set of typical offline kinematic requirements, applied at the Monte-Carlo truth level. Simulated data with pile-up for a luminosity of $\mathcal{L} = 5 \times 10^{32}$ cm^{-2}s^{-1}.

5 Summary and outlook

We have presented detailed descriptions of the algorithms that form the basis of an efficient (mini-)Level-1 trigger: the VELO tracking including primary vertex finding, TT1 tracking and matching to VELO track seeds, with determination of the transverse momentum, and finally a simple decision logic based on the impact parameters and transverse momenta of two selected tracks in the event.

The TT1 tracking station plays a central role in this concept and significantly improves the performance of the Level-1 trigger. We have studied two implementations of this detector, a straw-tube/silicon hybrid version and a full-silicon design, with regard to trigger performance and come to the conclusion that a full-silicon implementation of this tracking chamber improves the trigger efficiency, at the same minimum-bias retention rate, by 20–50% relative to the hybrid solution, depending on the signal channel. Conversely, it gives a minimum-bias retention rate that is lower by a factor of about two at equal signal efficiency.

This difference in the performance can be traced back mainly to the better resolution of the silicon detector, but also to the finer y-segmentation as well as to other small differences in the lay-out.

References

[1] The LHCb Collaboration, LHCb Technical Proposal, CERN/LHCC 98-4.

[2] P. Bartalini et al., *Tuning of Multiple Interactions Generated by* PYTHIA, LHCb/99-028, PHYS.

[3] F. Fiedler, *Super-Level1*, LHCb/2002-012, TRIG.
N. Tuning, *Tuning the Super Level 1 algorithm to the VELO-TDR geometry*, LHCb/2002-028, TRIG.

[4] F. Teubert, *How useful is to have momentum information at L1?*, talk given at LHCb-week meeting, 20 September 2001, `http://documents.cern.ch/cgi-bin/setlink?base=agenda&categ=a01632&id=a01632s1t7/transparencies`.

[5] The LHCb Collaboration, LHCb VELO Technical Design Report, CERN/LHCC 2001-011.

[6] Y. Ermoline, V. Lindenstruth, A. Walsch, *LHCb Level-1 Vertex Topology Trigger*, LHCb/99-031, TRIG.

[7] F. Teubert, I.R. Tomalin and J. Holt, *The LHCb Level-2 Trigger*, LHCb/98-047, TRIG.

[8] The LHCb Collaboration, LHCb Outer Tracker Technical Design Report, CERN/LHCC 2001-024.

[9] M. Needham, *TT1 layout and occupancies*, talk given at LHCb-light general meeting, 3 May 2002, `http://documents.cern.ch/cgi-bin/setlink?base=agenda&categ=a02410&id=a02410s5t2/transparencies`.

[10] M. Needham, *Inner and outer tracker occupancies in the light LHCb detector*, LHCb/2002-032.